21 Embryonic and neonatal morphology and ontogeny of a new species of *Hypacrosaurus* (Ornithischia, Lambeosauridae) from Montana and Alberta

JOHN R. HORNER AND
PHILIP J. CURRIE

Abstract

Cranial and postcranial elements of embryonic and nestling specimens are described from Alberta and Montana, for a new lambeosaurid species named *Hypacrosaurus stebingeri*. Ontogenetic changes between embryonic and nestling individuals include incipient development of the nasal crest, increase in the rows of teeth, changes in the proportion of the orbits to skull size, deepening of articular rugosities at union junctions, and changes in osteohistological structures. For the majority of elements, the morphology of the nestlings resembles that of the adults. Circumference-to-length ratios of the femora and tibiae change during ontogeny, with the elements becoming less robust with age. Worn teeth of the embryos indicate that these animals ground their teeth in the eggs, and that the teeth were functional upon hatching. Histological studies show that this species experienced very rapid growth during its nest-bound period. Phylogenetically, *Hypacrosaurus stebingeri* appears to be an intermediate taxon between a species of *Lambeosaurus* and *Hypacrosaurus altispinus*.

Introduction

Baby dinosaurs and dinosaur eggs have long been a source of fascination to both paleontologists (Jepsen, 1964) and the public (Andrews, 1932). The first reports of embryonic dinosaurs were from alleged protoceratopsian eggs found in Mongolia (Andrews, 1932). Although these reports have not been substantiated by further preparation of the eggs, embryonic bones of *Protoceratops* were nevertheless recovered by the American Museum of Natural History expedition (Brown & Schlaikjer, 1940). Embryonic remains of an unknown dinosaur were also reported from the eastern Gobi by Sochava (1972). Additional undescribed embryonic bones from central Asia were collected by the Canada–China Dinosaur Project and the Soviet–Mongolian Expeditions (see also Carpenter & Alf, Chapter 1).

In 1955, C. M. Sternberg described a small "hadrosaurine" skull that he referred to as a very young individual. Size comparison with embryonic specimens from Devil's Coulee suggests that the specimen (CMN 8917) is small enough to have been either embryonic or nepionic (postembryonic) when it died. Other isolated bones from the Judith River Formation of Alberta and Montana in the collections of the Royal Tyrrell Museum of Palaeontology, Canadian Museum of Nature, Museum of the Rockies, University of California at Berkeley, The Academy of Natural Sciences in Philadelphia (see Fiorillo, 1987), and the Yale Peabody Museum (Princeton Collections) clearly represent embryonic, hatchling, or nestling "hadrosaurs."

The Two Medicine Formation of northern Montana and southern Alberta has yielded an abundance of baby dinosaur remains (Horner & Makela, 1979), primarily found on nesting horizons (Horner 1982 and Chapter 8). A new species of *Hypacrosaurus* (see Appendix 1) is represented by the largest collection of baby material from the uppermost part of the Two Medicine Formation. Three nesting horizons, one in Alberta and two in Montana (Fig. 21.1) have yielded numerous eggs and the remains of baby individuals ranging from embryos to large nestlings (Currie & Horner, 1988). Juvenile and adult remains of this species are also very common.

Geological setting

All of the described and referred specimens, including the holotype of this new species of lambeosaurid, were found in the uppermost 100 of the 650-m thick Two Medicine Formation. A bentonite located within a few meters of the Devil's Coulee sites has been dated at 75.05 $\pm$0.08 Ma (D. Eberth & A. Deino, personal communications, 1992). The nests and isolated bones from Montana and Alberta were found in greenish-grey mudstones, some of which contained abundant caliche. Terrestrial gastropods and small wood fragments are common on the Montana nesting horizons.

Specimens

Specimens from Montana were derived from two major nesting horizons (see Horner, Chapter 8). One of

the horizons, located near Landslide Butte, Glacier County, extends for approximately 3 km. Hundreds of skeletal elements have been found, many associated with crushed eggs. None of the specimens represent individuals larger than 1 m in length. Sites along this horizon include Egg Baby Butte (MOR Locality Number TM-035), Egg Baby West (MOR TM-036), Baby Slide (MOR TM-037), Egg Explosion Hill (MOR TM-038), North Dome (MOR TM-039), and Egg Baby North (MOR TM-051). Specimens were found strewn randomly on the nesting horizon at each of these sites (Horner, Chaptrer 8). No associated skeletons were found, although a few associated but crushed eggs were collected.

Another nesting horizon, located on Blacktail Creek, Glacier County (MOR TM-066), yielded a nest

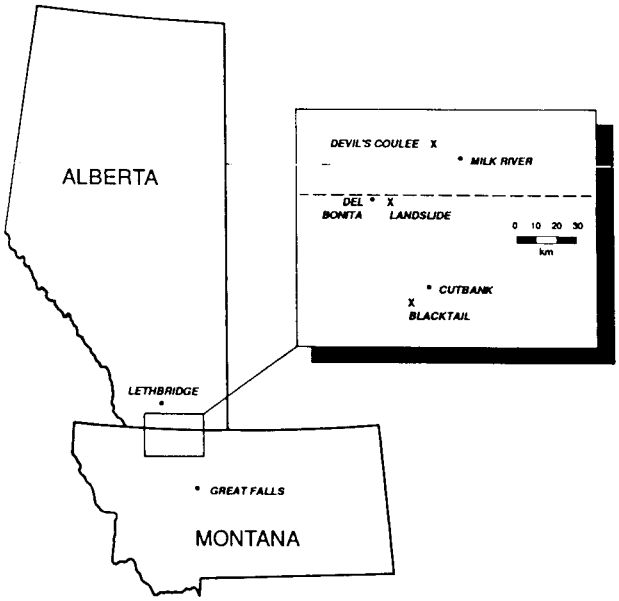

Figure 21.1. Map of Montana and Alberta showing geographic relationship of nest localities.

Figure 21.2. *Hypacrosaurus stebingeri*. Map of egg clutch from Devil's Coulee (RTMP 89.79.53).

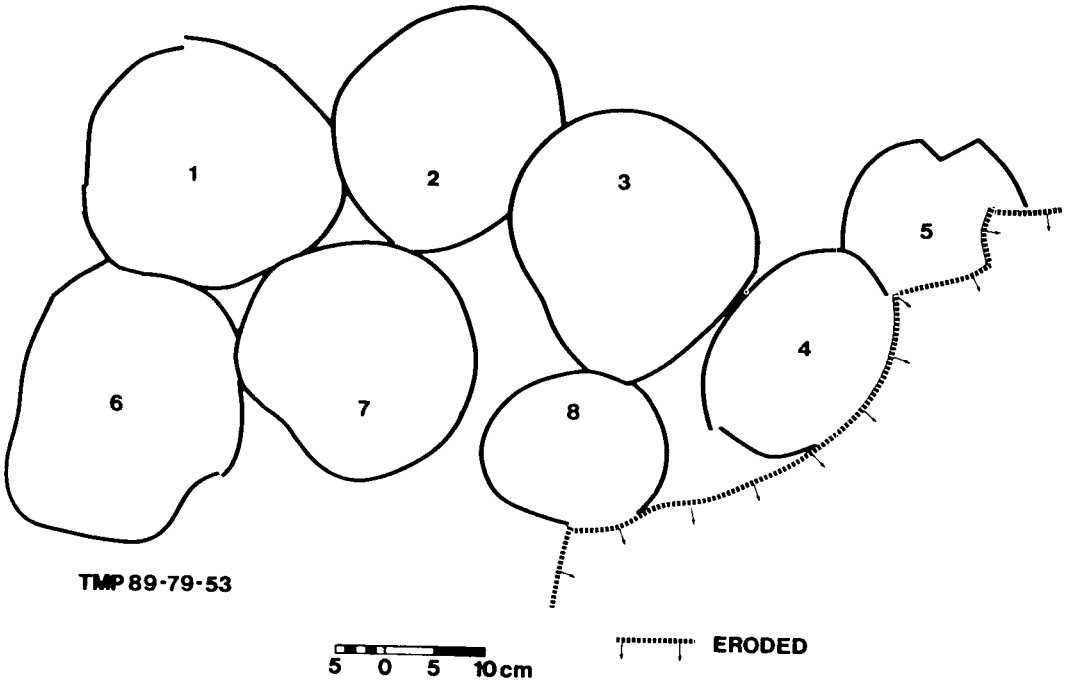

with broken eggs, a clutch of eggs with embryos (MOR 559), and a fluvial concentration of disarticulated skeletal remains (MOR 548) representing at least twelve individuals. An isolated embryonic or nepionic individual (MOR 562) was collected from Badger Creek, Glacier County (TM-065S).

Devil's Coulee in southern Alberta has yielded several nests from a variety of sites. Most of the specimens used in this study of embryonic individuals came from a single nest (No. 2) at a locality known as Little Diablo's Hill. Four eggs (RTMP 88.79.36) excavated from Nest No. 2 have not been prepared, but embryonic bones were seen in at least one of the broken eggs at the time they were collected. Disarticulated bones from broken eggs at the edge of the nest represent at least three individuals, and other bones washed out of the nest by recent erosion were cataloged under accession number RTMP 87.79. A single associated individual, RTMP 89.79.52, was recovered from another part of the nest.

Little Diablo's Hill has yielded four additional nests, two of which contain embryonic specimens, whereas the remaining two contain eggs without embryonic material. One of these nests (RTMP 89.79.53) contained eight eggs (Fig. 21.2). The eggs are large and almost round. A reconstruction (RTMP 90.130.1) of an egg from the nest measures 18.5 × 20 cm and has a volume of 3,900 ml. Erosion had destroyed one side of the nest so the original clutch size is unknown. Two other sites in Devil's Coulee (North Baby Butte and Kiddie's Corner) have also yielded embryonic material.

The embryonic and nestling material from Montana is in relatively good condition, although some cranial elements such as the premaxillae have been crushed. In contrast, nearly all of the embryonic material from Devil's Coulee is uncrushed and in very good condition.

Cranial morphology

Every bone of the skull, except the supraoccipital and the vomer, have been identified among the embryonic material from Devil's Coulee. Some elements, however, are hidden from view within articulated skulls. The estimated skull length of RTMP 89.79.52 is 7.5 cm (Figs. 21.3 & 21.4). For the large nestling, all the major cranial elements are known except the vomer, pterygoid, ectopterygoid, angular, splenial, and articular. The composite skull of nestling MOR 548 from Blacktail Creek, Montana, is 20 cm in length (Fig. 21.5). For descriptive convenience the skulls of the embryos and nestlings are divided into the segments (complexes) originally defined and used by Ostrom (1961).

Neurocranial complex

The parietals of the smallest embryos show no midline suture between left and right sides. Embryonic specimens of *Maiasaura peeblesorum* also show no sign of a midline suture. This suggests that the bone formed from a single ossification center in contrast with the ancestral state of reptiles, in which the parietals are paired (Weishampel & Horner, 1990). The embryonic parietal (RTMP 87.79.241) of the hypacrosaur is broader than long and broadly expanded (Fig. 21.6). A strong midline ridge separates the squamosals posteriorly, but this ridge does not extend anteriorly into a sagittal crest. The anterior margin of the parietals are notched on the midline, presumably a center for growth that is not seen in mature individuals (Gilmore, 1937). The posterior ends of the frontals overlapped onto a digitated ledge on the anterolateral surfaces of the parietals. In the nestlings (MOR 548) the parietal remains broad but has developed a relatively high sagittal crest (Fig. 21.7 A,B). Two posteroventral processes of the parietals attach to the dorsal surface of the supraoccipital, and the posterior

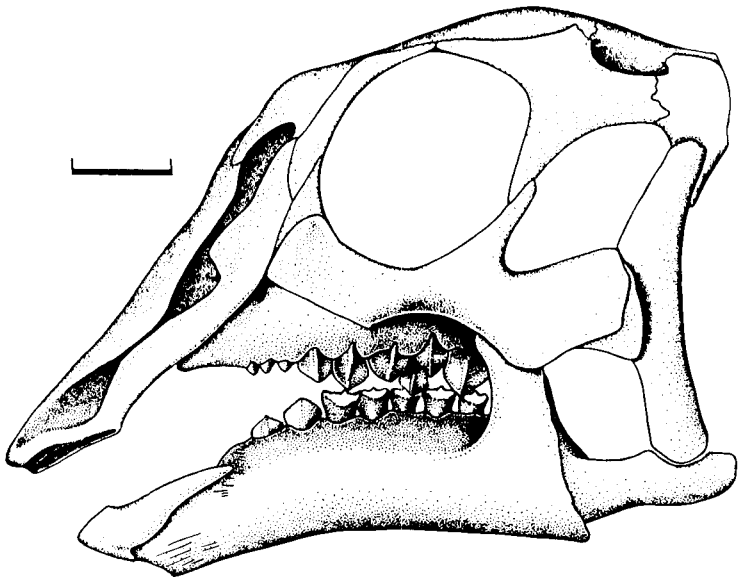

Figure 21.3. *Hypacrosaurus stebingeri.* Reconstruction of embryonic skull based on RTMP 89.79.52, RTMP 87.79.206 (frontal), RTMP 87.79.241 (parietal), RTMP 87.77.92 (prefrontal) and RTMP 87.79.333 (postorbital). Scale bar = 1 cm.

end of the posterodorsal process extends between the squamosals. The anterior ends of the parietals of the nestlings are more rugose where the frontals meet than those of embryonic specimens.

The embryonic frontal (Fig. 21.8) is thickened laterally where it meets the prefrontal and postorbital. There is a distinct posterolateral depression on the ventral side that received a portion of the postorbital condyle of the laterosphenoid. In hadrosaurids, the postorbital condyle of the laterosphenoid does not contact the frontal (Horner, 1992). The medial edge of the embryonic frontal is extremely thin, and there is no evidence of a sutural union. There may actually have been an unossified region between the paired elements. In the

Figure 21.4. *Hypacrosaurus stebingeri*. **A**. RTMP 89.79.52, enlargement of left maxillary tooth, labial view. **B**. RTMP 89.79.52 in left lateral view. **C**. RTMP 89.79.52 in right lateral view. **D**. Right squamosal in external view. **E**. Right squamosal in internal view. Abbreviations: an, angular; ar, articular; b, basioccipital; bs, basisphenoid–parasphenoid complex; d, dentary; ec, ectopterygoid; eo, exoccipital; h, hyoid; j, jugal; ls, laterosphenoid; m, maxilla; n, nasal; pal, palatine; pd, predentary; pm, premaxilla; po, postorbital; pr, prootic; prf, prefrontal; pt, pterygoid; q, quadrate; sa, surangular.

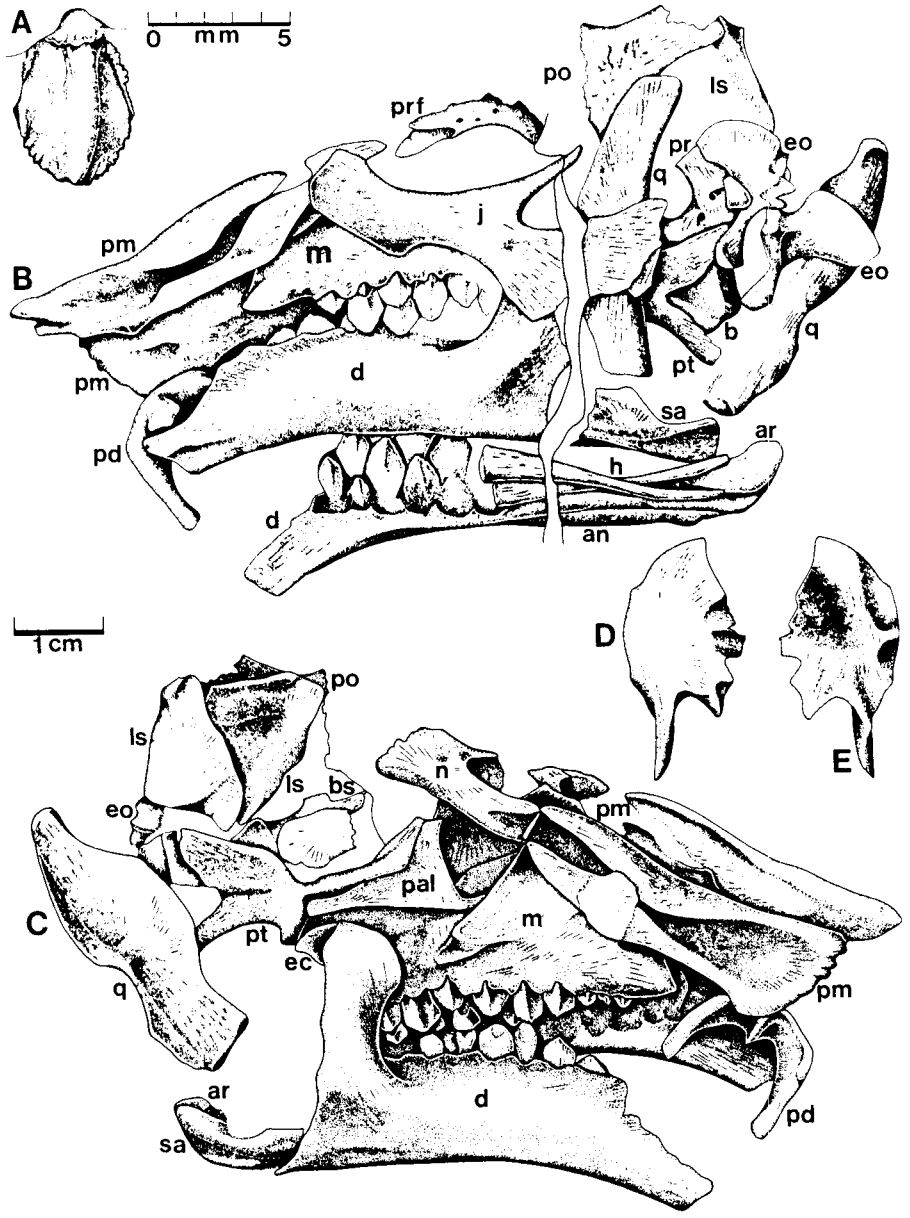

nestlings (Fig. 21.7C), the medial surface is thickened and slightly interdigitated where it clearly unites the elements. In both the embryonic and nestling individuals, the frontals are greatly excavated ventrally and domed dorsally as in other juvenile lambeosaurids. The frontal surface for union with the nasal is indistinct in the embryonic specimen, but very distinct in the nestling and all juveniles.

The supraoccipital of the nestling (Fig. 21.7D) is almost identical to the supraoccipital of juvenile or adult lambeosaurids (see Gilmore, 1937; Langston, 1960), except that the supraoccipital bosses are poorly developed, and the shelf over the foramen magnum is extremely short. The supraoccipital contacts the squamosals and parietals laterally, the exoccipitals ventrolaterally, and the prootic anterolaterally. Within the anterolateral process, which contacts the prootic, is an opening that represents the dorsoposterior end of the otic vestibule. In the nestlings, the nuchal notch, located posteriorly between the supraoccipital and parietal, is an opening that extends from the posterior end of the brain cavity to the exterior surface of the skull. This notch closes with maturity.

The exoccipitals (Figs. 21.7E and 21.9) apparently fuse with the opisthotics early in embryonic development, because there is no evidence of a suture between them as has been suggested by Langston (1960). As in hadrosaurids, the exoccipital unites with the squamosal, supraoccipital, basioccipital, prootic, and basisphenoid. An extremely narrow wing contacts the paired exoccipitals on the midline of the posteroventral surface of the supraoccipital. On the anterodorsal surface of the basisphenoid process is located the opening to the posterior end of the otic vestibule. This opening is particularly large in the embryos and nestlings, suggesting that the babies had a very good sense of hearing.

The basioccipital (Figs. 21.7G and 21.10) is an indistinct flattened element with a broad, slightly concave depression that forms the base of the brain cavity. The basioccipital unites with the exoccipitals, prootics, and basisphenoid. The floor of the foramen magnum is proportionately very broad in both the embryonic and nestling individuals.

The prootic (Figs. 21.7H and 21.11) attaches to the anterior margin of the exoccipital and to the basioccipital, supraoccipital, laterosphenoid, and basisphenoid. The posterior end of the prootic houses the anterior end of the otic vestibule (Fig. 21.11). Anteriorly, the prootic is excavated where it forms the posterior wall of the trigeminal foramen (cranial nerve V, Fig. 21.4B). In the embryos, this opening is relatively much larger than in mature individuals. The foramen for cranial nerve VII also penetrates the prootic. Between the posterior end of the prootic and the anteroventral end of the exoccip-

Figure 21.5. *Hypacrosaurus stebingeri*, composite skull of MOR 548 in right lateral view. Scale in centimeters.

ital is located a large open area that was apparently occupied by cartilage and the fenestra ovalis (Langston, 1960).

The laterosphenoid (Figs. 21.4, 21.7I, and 21.12) unites with the prootic, basisphenoid, frontal, postorbital, parietal, orbitosphenoid, and in larger specimens, the opposite laterosphenoid. In the embryos (Figs. 21.4, 21.12), the laterosphenoid is a triangular, platelike bone with a postorbital process that is short relative to those of mature specimens. The posteroventral angle forms the anterior margin of the trigeminal foramen and is separated from the rest of the bone by a deep groove for the ophthalmic branch of the trigeminal. The laterosphenoid of the nestling (Fig. 21.7I) has much the same morphology as in the mature specimens. The dorsal process of the laterosphenoid fits into a socketlike depression on the ventral surface of the postorbital and frontal. In hadrosaurids this union is restricted to the postorbital (Horner, 1992).

The basisphenoid and parasphenoid are united to form a single element, herein referred to as the parasphenoid–basisphenoid complex (Figs. 21.7F, 21.13). Fusion of the two bones apparently occurred very early in embryonic development, because they are fused in the smallest embryonic individuals. This complex unites with the laterosphenoids, prootics, opisthotics (exoccipitals), basioccipital, and pterygoids. It forms the ventral margin of the trigeminal foramen and plays a minor role in the formation of the fenestra ovalis. The sella turcica is deep and well demarcated.

Figure 21.6. *Hypacrosaurus stebingeri*. RTMP 87.79.241. Embryonic parietals in ventral and dorsal views. 1, frontal suture. Top is anterior. Scale = 5 mm.

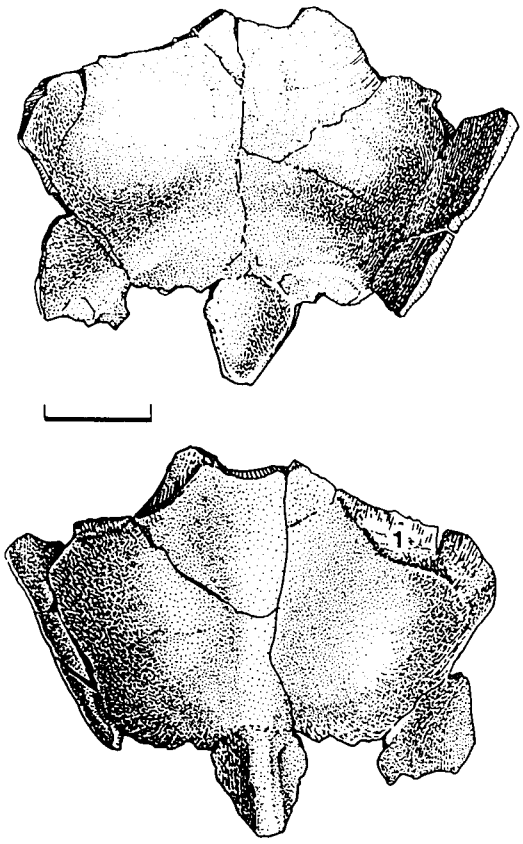

Shallow canals on either side of the dorsum sellae mark the passage of the sixth cranial nerves, which passed out of the braincase anteromedial to the laterosphenoid–basisphenoid suture. The basipterygoid processes are broken in RTMP 87.79.335, but they appear to have been relatively shorter than those of nestlings, juveniles, and adults. The suture with the basioccipital is transverse, but the basioccipital is also supported by a pair of short, posteriorly directed processes in the position of the basal tubera. The cultriform process is U-shaped in section where it supported the interorbital septum, and it is separated from the pituitary region by a distinct step.

The round orbitosphenoid attaches to the anterior edge of the laterosphenoid. It also attaches to the frontal, the presphenoid, and the opposite orbitosphenoid. The nestling orbitosphenoid (Fig. 21.7J) is a subrounded, flattened bone that is pierced by two foramina apparently for cranial nerves III and IV. A wall for the foramina of cranial nerve II most likely bordered the element (see Horner, 1992).

None of the ethmoids appear to have been ossified in the embryonic specimens. They were not found nor identified in the nestlings as well.

Maxillary complex

The premaxilla (Figs. 21.4, 21.14A,B, & 21.15) is one of the largest bones in the skull, even though it is relatively smaller compared to the skull than in mature individuals. The attachment surface for the keratinous bill (ramphothaeca) is a distinct transverse groove with dorsal projections located along the anterior border of the premaxilla (Fig. 21.15). The nasal groove is restricted just posterior to the external nares, similar to *Hypacrosaurus altispinus*. Posteriorly, the groove expands, then constricts before meeting the nasal. There is a distinct tapering process on the posteromedial end of the premaxilla. The lateral surface of this process meets the medial side of the nasal. The lateroventral process of the premaxilla meets the anterolateral end of the nasal.

One of the few differences between the embryonic and nestling premaxillae is the presence of an anteriorly directed excavation on the posteroventral surface of the nestling premaxilla. This excavation resides between the dorsal and ventral posterior processes and apparently represents the initial development of the S-loop (Weishampel, 1981a). The nestling premaxilla also clearly shows a pair of shallow grooves that extends anteriorly along the medial surface from the premaxil-

lary–nasal union. The dorsal groove extends anteriorly to the attachment groove for the ramphothaeca. The ventral groove passes down and exits on the ventromedial surface of the premaxilla. These grooves, distinct in juveniles and adults, apparently carried vessels and nerves to the keratinous bill and to the roof of the anterior end of the mouth.

The maxilla of both embryos and nestlings is basically triangular in lateral aspect (Figs. 21.4, 21.14D, and 21.16). The apex of the triangle, at the dorsal limit of the jugal suture, is approximately one third the distance from the anterior margin of the maxilla in the embryo. The apex in juveniles and adults is located in the middle of the maxilla. The premaxillary shelf of the maxilla is angled downward very steeply in the embryos (47°) and nestlings (42°). In adults, this angle is about 30°. Embryonic specimen RTMP 87.79.286 appears to have twelve rows of teeth over its 45 mm length. The nestlings have about twenty teeth in maxillae, which average 85 mm in length. As in mature individuals, the teeth of the nestlings are closely packed, although the packing is looser because the teeth being shed are smaller than those replacing them. The largest teeth in the embryonic maxillae average about 4 mm in anteroposterior length (Fig. 21.4A). The teeth have several marginal denticles on both the anterior and posterior edges. The nestling teeth are about 5 mm in length, and show only a slight indication of marginal denticles.

The jugal of the embryo (Figs. 21.4, and 21.17) has an elongate maxillary process and a very broad orbital margin. The jugal of the nestling (Fig 21.14E) is almost identical to the jugal of an adult *Hypacrosaurus altispinus* (Gilmore, 1924), except that the orbital margin remains proportionately larger in the nestling. In addition, the anterior process is not as anteroposteriorly compressed, and the postorbital process is more elongate than in the adult.

The quadratojugal of the nestling (Fig. 21.14F) is a thin triangular bone with a characteristic anteroventrally projecting jugal process. The medial side of the quadratojugal fits like a flap over the quadratojugal notch in the quadrate. The quadrate is nearly covered

Figure 21.7. *Hypacrosaurus stebingeri*. MOR 548. **A**. Parietal in dorsal view. **B**. Parietal in left lateral view. **C**. Right frontal in dorsal view. **D**. Dorsal view of supraoccipital (D). **E**. Posterior aspect of exoccipitials. **F**. Left lateral view of basisphenoid. **G**. Dorsal view of basioccipital (anterior left). **H**. Lateral view of left prootic. **I**. Lateral view of left laterosphenoid. **J**. Lateral aspect of left orbitosphenoid. Scale = 4 cm.

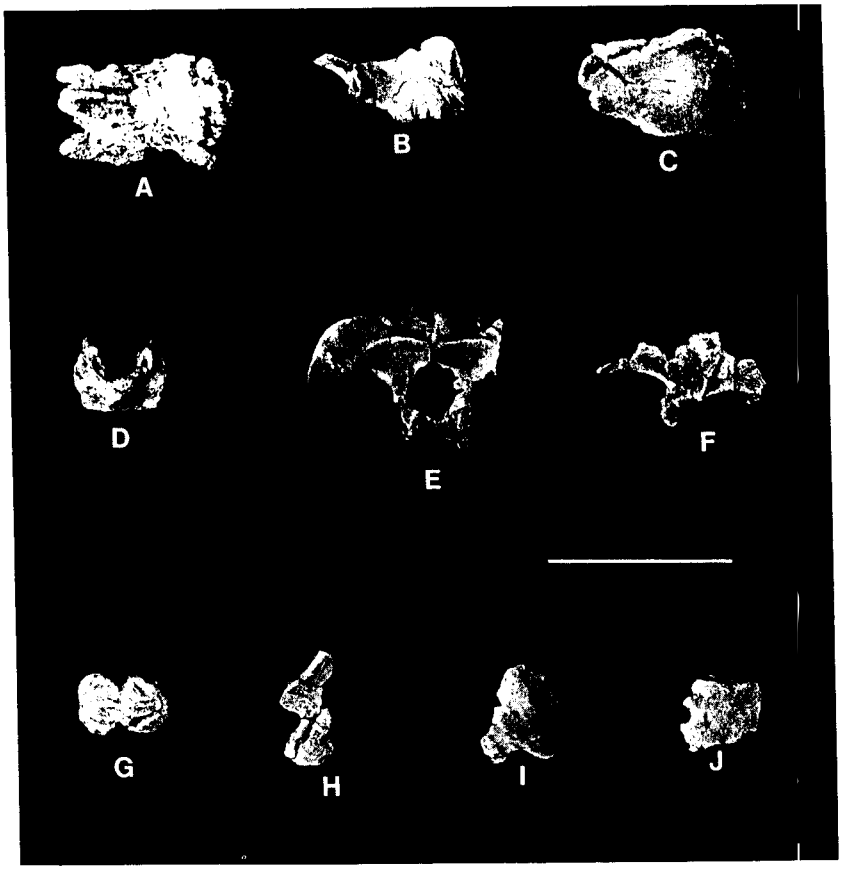

by the quadratojugal in the embryonic RTMP 89.79.52 (Fig. 21.4B).

The quadrates of the embryos and nestlings (Figs. 21.4, 21.14G, and 21.18) are nearly identical with the corresponding adult quadrates. The only differences are that the embryonic specimen has a much less distinctive quadratojugal notch and articular condyle.

The squamosals of embryos and nestlings (Figs. 21.4B,C, and 21.14H) are very similar to those of the adults but do not form as broad a roof over the posterior portion of the supratemporal fenestra. This condition is, however, variable among the nestlings. The embryonic squamosal is thin along most margins, and the contact with the supraoccipitial has not developed into the pronounced process seen in juveniles and adults.

The postorbital of the embryo (Fig. 21.19) is similar to that of the nestling (Fig. 21.14I), except that the prefrontal and frontal processes are not nearly as broad or rugose. In the embryo, the prefrontal process of the postorbital is pointed and thin, whereas in the nestling it is blunt and thickened. Also in the nestling the posterior wall of the orbit is much broader than in the embryo. Both the postorbital and squamosal processes are similar in the embryos and nestlings, although in the nestling these processes possess much more distinctive articulations. One difference between the embryos and nestlings is the embryo's proportionally smaller supratemporal fenestra. In the nestlings, the fenestra is proportionally similar to mature individuals.

The prefrontal (Figs. 21.4B, 21.14J, and 21.20) is an elongated bone with a slightly raised medial rim. A longitudinal groove along the median side receives the lateral edge of the nasal. A shallow V-shaped groove on the anterolateral end of the bone receives the lacrimal. On the anteromedial end of the bone is a shallow longitudinal groove that receives the posterior end of the premaxilla. In mature individuals, the medial rim of the prefrontal is very steep where it laps onto the expanded premaxillae of the nasal crest (Gilmore, 1937). The prefrontal becomes foreshortened with maturity. At least one foramen penetrates the orbital rim of the prefrontal. In juvenile lambeosaurids, the entire medial face of the prefrontal rests on the posterolateral surface of the nasal. In hadrosaurids, the medial surface of the prefrontal is separated into dorsal and ventral surfaces by a longitudinal ridge. The dorsal surface receives the nasal, and the ventral surface forms the lateral wall of the internal nares (Horner, 1992).

The lacrimal is a triangular bone in both the embryos and nestlings (Fig. 21.14K). It contacts the premaxilla, maxilla, jugal, and palatine. In juveniles and adults, the lacrimal becomes more elongate and narrows anteroventrally as the crest develops.

RTMP 89.79.52 includes most of the left nasal,

Figure 21.8. *Hypacrosaurus stebingeri*. RTMP 87.79.206. Left frontal in dorsal and ventral views. Laterosphenoid suture (1). Scale = 5 mm.

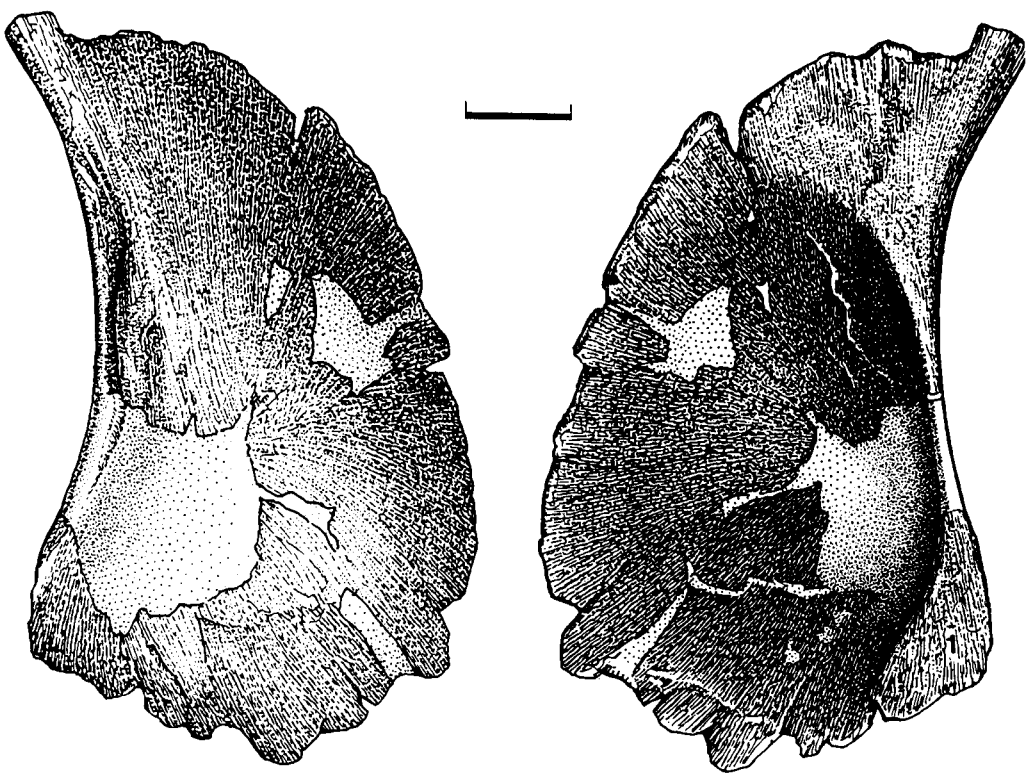

Figure 21.9. *Hypacrosaurus stebingeri*. RTMP 87.79.307. Left exoccipital–opisthotic. **A**. Posterior view. **B**. Dorsolateral view. **C**. Anterior view. **D**. Medial view. Supraoccipital contact (1); prootic suture (2). Scale = 5 mm.

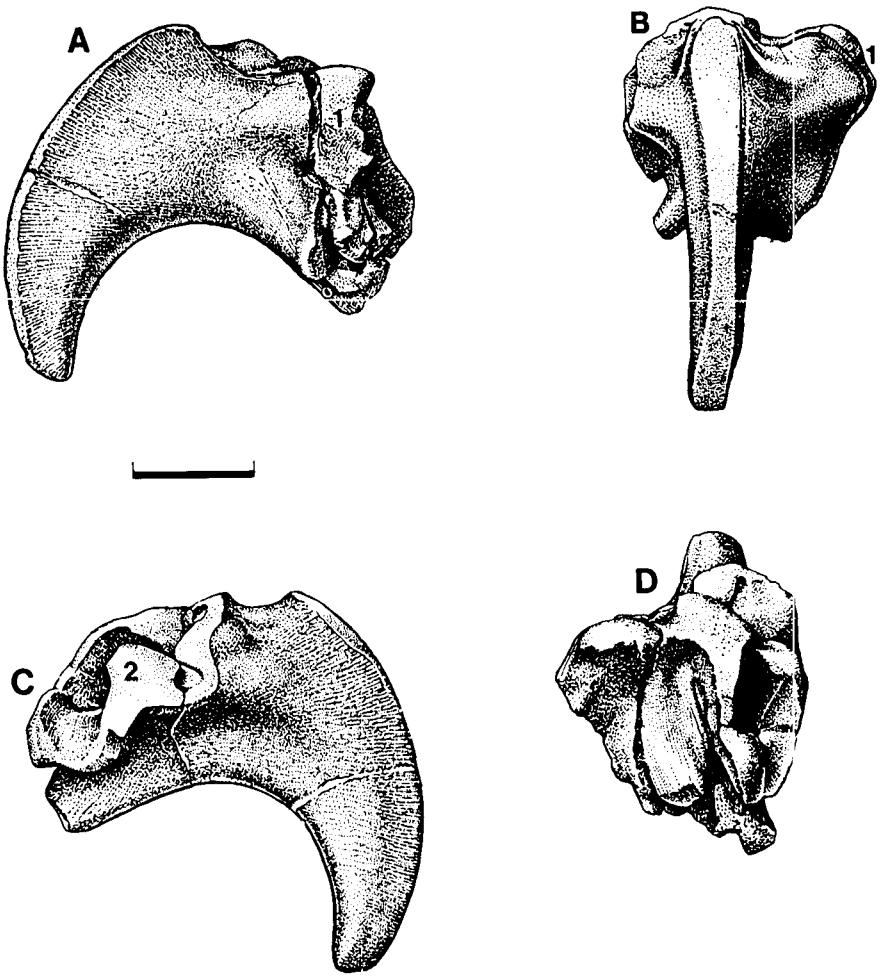

Figure 21.10. *Hypacrosaurus stebingeri*. RTMP 87.79.157. Basioccipital. **A**. Ventral view. **B**. Posterior view. **C**. Dorsal view. Basisphenoid contacts (1); exoccipital suture (2); prootic suture (3); occipital condyle (4). Scale = 5 mm.

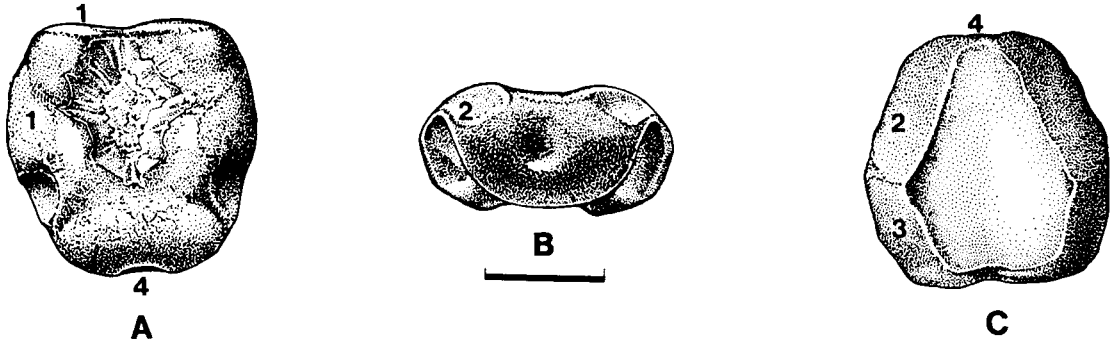

which has been flipped over and exposed on the right side of the skull (Fig. 21.4C). Anteriorly, a pair of processes form the posterior margin of the narial opening. The shorter lateroventral process is largely covered by the premaxilla, whereas the more extensive anteromedial process has a complex, forked contact with the premaxilla. In both the embryo and nestling (Fig. 21.14C), the nasal is a flattened, elongated bone that has a concave ventral surface and shows slight convexity on the dorsal surface posterior to the external narial boundary. The paired nasals are separated anteriorly by a pair of dorsoposterior processes of the premaxillae. In larger specimens, the lateral margin of the nasal is a smooth, ventrolaterally angled surface that is sutured to the prefrontal. The ventral surface of the posterior process rests on the anterodorsal shelf of the frontal.

Figure 21.11. *Hypacrosaurus stebingeri*. RTMP 87.79.201. Left prootic in posterior aspect. Otic vestibule (ov). Scale = 5 mm.

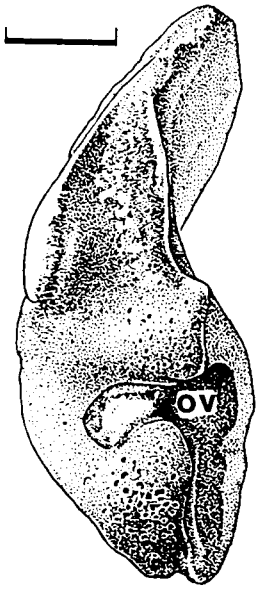

The embryonic pterygoid (Fig. 21.4B,C) is similar to that of other lambeosaurids but is relatively longer and lower than in mature individuals. The saddlelike groove (Heaton, 1972) is more pronounced, and the dorsal margin of the posterior alar projection is more arched in lateral view. The sutural contact with the palatine is not fused.

The embryonic ectopterygoid (Figs. 21.4 and 21.21) is an elongate, gently curving bone that separates the pterygoid from the maxilla. The distinctive lambeosaurid shape is already established in the ectopterygoid even at this stage of development. The medial surface is divided by a sharp but thin ridge into an elongate dorsal surface that posteriorly contacts the pterygoid and a ventral concavity for the maxilla. The posteroventral end of the ectopterygoid is wrapped around the ventral end of the ectopterygoid ramus of the pterygoid.

The embryonic palatine (RTMP 89.79.52) is exposed in labial view (Fig. 21.4C) and is relatively longer and shorter than the same element of mature lambeosaurids (Heaton, 1972). The ventral margin is almost straight, rather than convex in ventral outline, and rests on the median, posterodorsal surface of the maxilla. The anterolateral flange of the nestling palatine (Fig. 21.14L) articulates with the ascending maxillary apex ventrally and apparently a very small portion of the jugal dorsally (Heaton, 1972). This junction is very different in hadrosaurids, and there is no junction of the palatine and lacrimal as in *Prosaurolophus* (Horner, 1992). Along the dorsal margin, on the posterior half of the palatine, is located a deep excavation for contact with the anterior end of the pterygoid. In the anterior half, a process extends medially, and together with the anteriormost end of the pterygoid forms the roof of the palate. As in hadrosaurids, the posterior process of the vomer fits between the anteriormost ends of the palatine and pterygoid (Horner, 1992). In lambeosaurids, the anterior pterygoid process rests on the dorsolateral surface of the

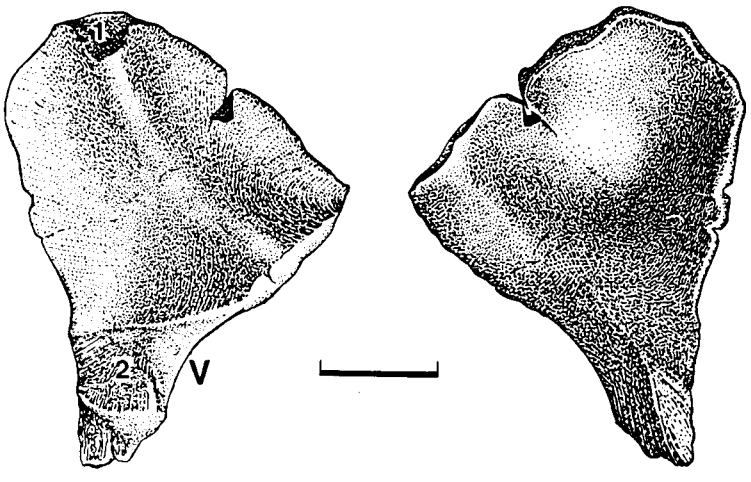

Figure 21.12. *Hypacrosaurus stebingeri*. RTMP 87.79.227. Right laterosphenoid in lateral and medial views. Postorbital articulation (1); groove for ophthalmic branch of trigeminal (2); anterior margin of opening for fifth cranial nerve (V). Scale = 5 mm.

medial process of the palatine, whereas in hadrosaurids the palatine rests on the anterior process of the pterygoid.

Mandibular complex

The predentaries of the embryo (Fig. 21.4B,C) and nestling (Fig. 21.22B) are identical in morphology and proportions to the corresponding element in juveniles and adults.

The embryonic dentary (Figs. 21.4B,C and 21.23) is similar in morphology to those of more mature specimens, although the ratio of height/length of the dental battery decreases with maturity. The paired dentaries of RTMP 87.79.266/267 are 54 mm long. There are eleven rows of teeth in the 41 mm long dental batteries, with two teeth per row. New rows are added at both the front and back of the battery and the antero-posterior crown lengths of unerupted teeth are less than 3 mm. In contrast, an unerupted tooth in the middle of the jaw is 5.2 mm long and 9.8 mm high. Most of the erupted teeth show occlusal tooth wear. The dentaries of RTMP 89.79.52 are shorter (49 mm), but the largest unerupted teeth are the same size as those of RTMP 87.79.266/267. The smallest embryonic dentary, RTMP 87.79.6, recovered from Nest No. 5 on Little Diablo's Hill, is less than 40 mm long and had only eight or nine rows of teeth. An embryonic jaw from nest MOR 559 has a length of 40 mm with eight tooth rows.

The nestling dentary (Fig. 21.22A) is very similar in morphology to the adult dentary, except that the ratio of height/length of the dental battery is deeper in the nestling. There are twenty rows of teeth within an 80 mm long dental battery. Two teeth per row are preserved, although the lower portion of the dental battery is crushed as is the case with most hadrosaurid and lambeosaurid jaws (Horner, 1983). The largest unerupted tooth, found in the midsection of the dentary, has a crown height of 14 mm and a crown antero-posterior length of 5 mm. The largest nestling dentary has 21 teeth in 90 mm. The largest teeth have a crown height of 17 mm and a length of 6 mm. The nestling teeth have little or no serrations along their anterior or posterior margins.

Surangulars of the embryos and nestlings (Figs. 21.4, 21.22C, D, 21.23) have proportions and morphology that are nearly identical to those of the juveniles and adults.

The splenial, angular, and articular are found in the embryonic mandibles (Figs. 21.4 & 21.23) and look much as they do in the juveniles and adults. The articular is a small, lateromedially thin bone between the splenial and surangular. As in more mature individuals, it makes only a small contribution to the jaw articulation.

A pair of hyoids (ceratobranchials) are preserved in RTMP 89.79.52 (Fig. 21.4). They extend from the back of the jaws to the coronoid region. In overall morphology, they are indistinguishable from those described in mature specimens of *Corythosaurus* (Ostrom, 1961) in being deep and flattened anteriorly and in tapering posteriorly.

Postcranial morphology

All bones of the postcranial skeleton are represented for the embryos (RTMP 89.79.52) and nestlings (MOR 548). However, none of the nestling pubii have complete anterior processes.

Axial skeleton

Vertebrae of baby hadrosaurids, such as *Maiasaura peeblesorum* and lambeosaurids, share several common features and a nearly identical early ontogeny. The centra have a notochordal pit on the anterior and posterior faces in both embryos and nestlings. In addition, embryonic and nestling hadrosaurids and lambeosaurids have proportionally large neural canals, the sizes

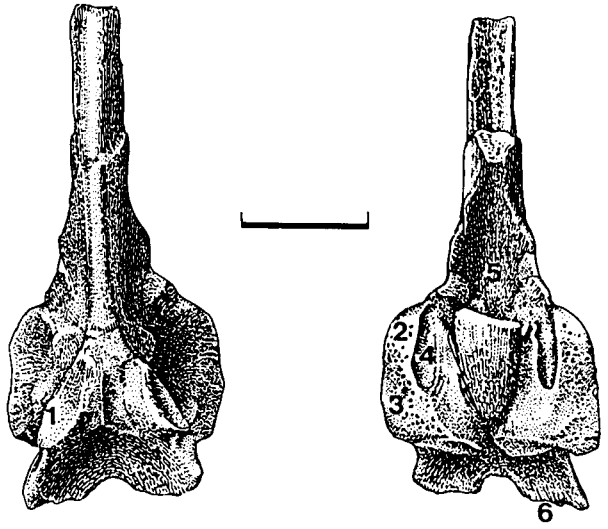

Figure 21.13. *Hypacrosaurus stebingeri*. RTMP 87.79.335. Parasphenoid–basisphenoid complex in ventral and dorsal views. Basipterygoid process (1); laterosphenoid suture (2); prootic suture (3); trough for sixth cranial nerve (4); sella turcica (5); basal tubera (6). Scale = 5 mm.

of which are age dependent. The sutural surfaces for the neural arches and transverse processes vary in degree of rugosity depending on the growth stage. Embryonic centra have shallow, smooth depressions for the neural arch and transverse processes, whereas large nestlings have shallow, slightly rugose sutural surfaces. These surfaces become progressively more rugose until finally coossification occurs.

The timing of fusion in the vertebrae is not the same throughout the column. In large nestlings, the cervical and dorsal neural arches are generally attached but are not yet fused; timing for fusion is not yet known. Fusion of sacral centra, on the other hand, occurs progressively beginning about the time the individuals are 2.5–3 m in length. The neural arches and transverse processes of sacrals do not begin to fuse until the juveniles are 3–4 m in length. Distal caudal arches begin to fuse when the individuals are about three meters in length.

The cervical vertebrae of the nestlings (MOR 548) have the features of the adult specimens (Figs. 21.24A, B). However, the neural canal is exceptionally

Figure 21.14. *Hypacrosaurus stebingeri*. MOR 548. **A**. Lateral view of the proximal half of the right premaxilla. **B**. Dorsal view of the distal half of the right premaxilla. **C**. Right nasal in dorsal aspect (anterior to left). **D**. Lateral view of right maxilla. **E**. Left jugal in lateral aspect. **F**. Lateral surface of left quadratojugal. **G**. Right quadrate in lateral view. **H**. Left squamosal. **I**. Postorbital. **J**. Prefrontal. **K**. Lacrimal. H–K shown in lateral aspects. **L**. Dorsal view of right palatine. Scale = 4 cm.

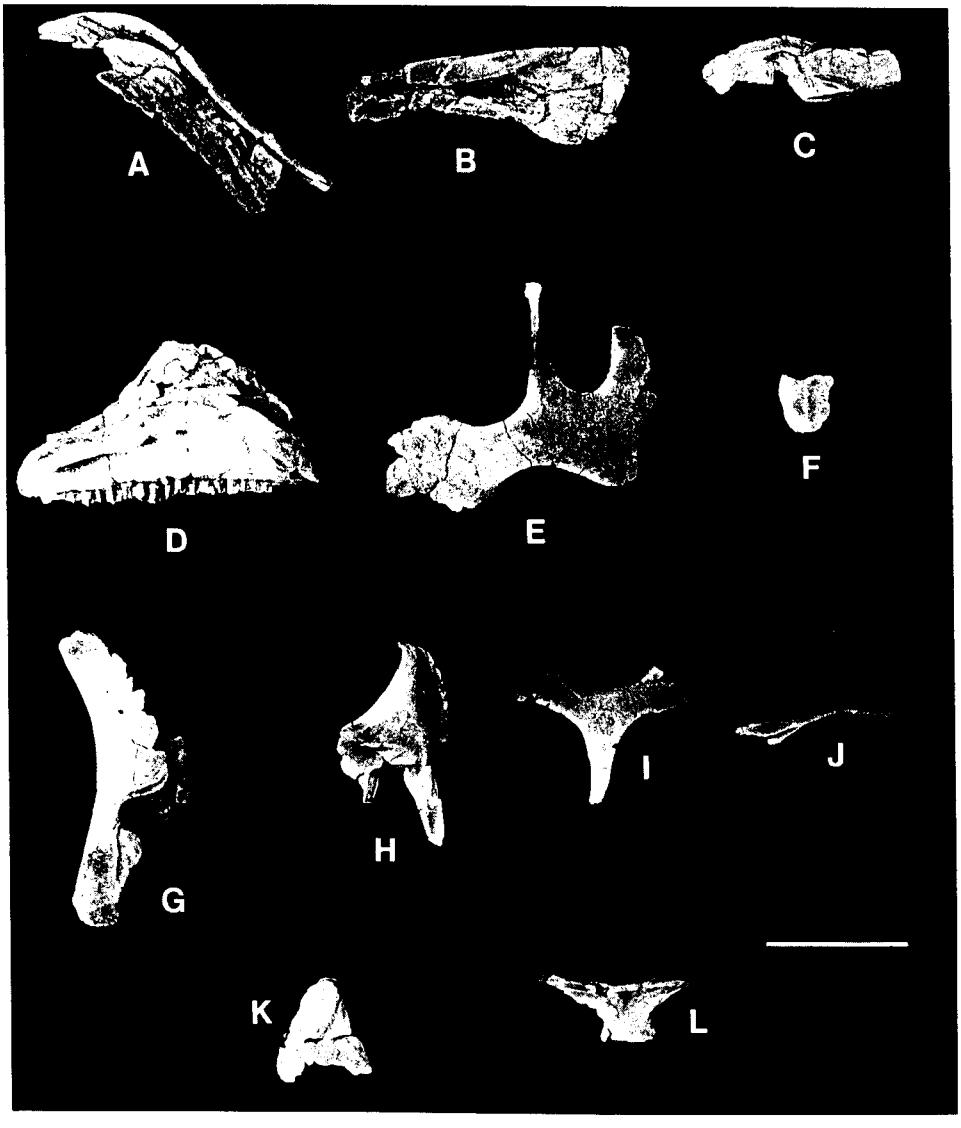

Figure 21.15. *Hypacrosaurus stebingeri*. RTMP 87.79.334. Right premaxilla in lateral, ventral, and dorsal views. Scale = 5 mm.

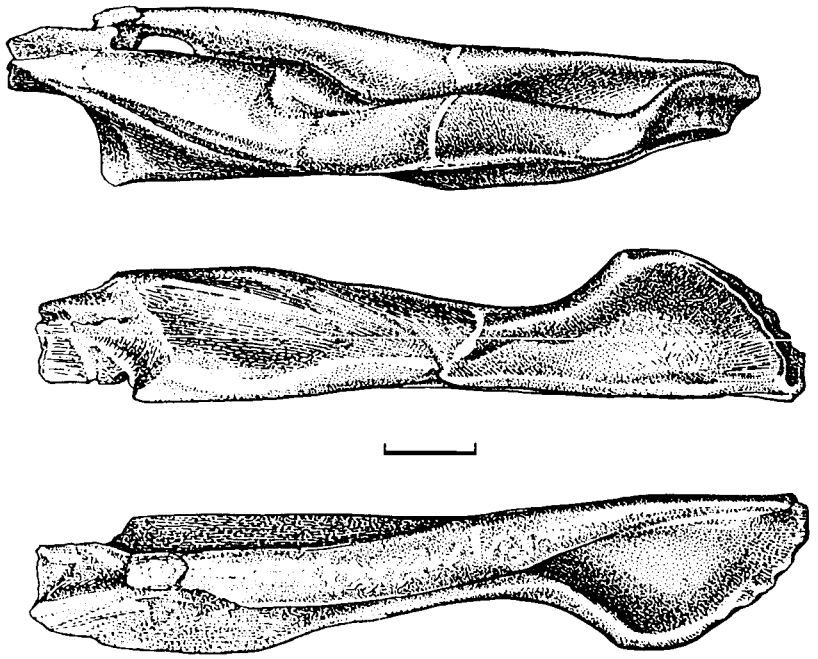

Figure 21.16. *Hypacrosaurus stebingeri*. RTMP 87.79.336. Left maxilla in medial and lateral views. Jugal suture (1); ectopterygoid contact (2). Scale = 5 mm.

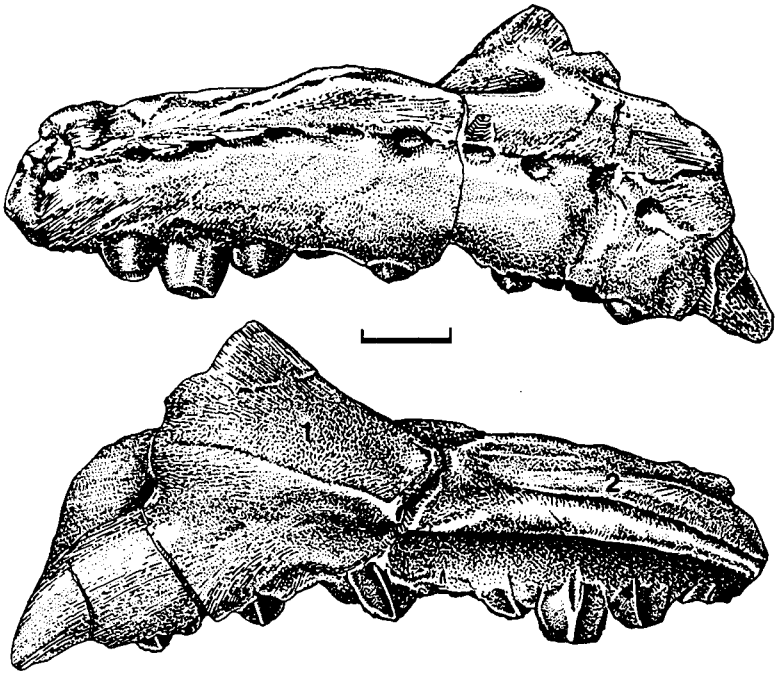

large in the anterior cervicals, and the zygapophyses are proportionally larger than in juveniles and adults. Proportions of the posterior cervicals of nestlings are nearly identical with the adults. In the embryo, the right and left halves of the axis (RTMP 87.79.242) are not co-ossified.

Like the cervicals, the dorsal vertebrae (Figs. 21.24C, D, E) have all of the morphological features found in the adults. The anterior dorsals have long diapophyses and neural spines that are proportionally much shorter those of adults. However, the neural spines of the nestlings are relatively broad anteroposteriorly. The posterior dorsals also have relatively short neural spines compared to the adult.

There is no fusion of the embryonic or nestling sacrum. Only five centra can be positively identified as sacrals (Fig. 21.24F, G, H). Two additional vertebral centra have expanded neural canal floors similar to the other sacrals and may represent the anteriormost and posteriormost sacrals of the juveniles. The adult sacrum consists of eight co-ossified vertebrae. The ventral surface of the nestling sacral centra have a median keel similar to adult lambeosaurids. All of the sacral parapophyses are disarticulated (Fig. 21.24I) and their relationships with their respective sacral vertebrae have not been determined. The sacral neural spines are very broad anteroposteriorly, and relatively high (Figs. 21.24G,H). The neural canal is exceptionally large, and becomes progressively smaller with maturity (Weishampel & Horner 1990).

The caudal vertebrae of the nestlings (Figs. 21.24J, K, L) have proportions similar to the adults. The neural spines are relatively long and broaden anteroposteriorly near their superior ends. The chevrons (Fig. 21.24M) are very long and taken together with the tall neural spines make a very deep tail.

The ribs of the embryos and nestlings (Fig. 21.26A) have the features and proportions of the adult ribs.

Appendicular skeleton

The scapula, coracoid, humerus, ulna, and radius of the embryos and nestlings (Fig. 21.25A) have a morphology similar to the adults. The smallest embryonic scapula (MOR 559S2), with a length of 30 mm, has an extremely narrow neck and enlarged articular facets. Proportions are more like the adult in larger embryos and nestlings. The nestling coracoid (Fig. 21.25B) is nearly identical to more mature specimens, although the anteromedial blade is somewhat thinner. Also, the coracoid foramen is not enclosed but is a narrow slit that splits the scapular and humeral articulation surface. The sternal of the embryo (RTMP 87.79.205) has a short, broad anterior blade, whereas in the nestlings the blade is narrower and more elongate (Fig. 21.25C) and is similar to that of the adult.

Figure 21.17. *Hypacrosaurus stebingeri*. RTMP 87.79.332. Left jugal in lateral and medial views. Maxillary suture (1). Scale = 5 mm.

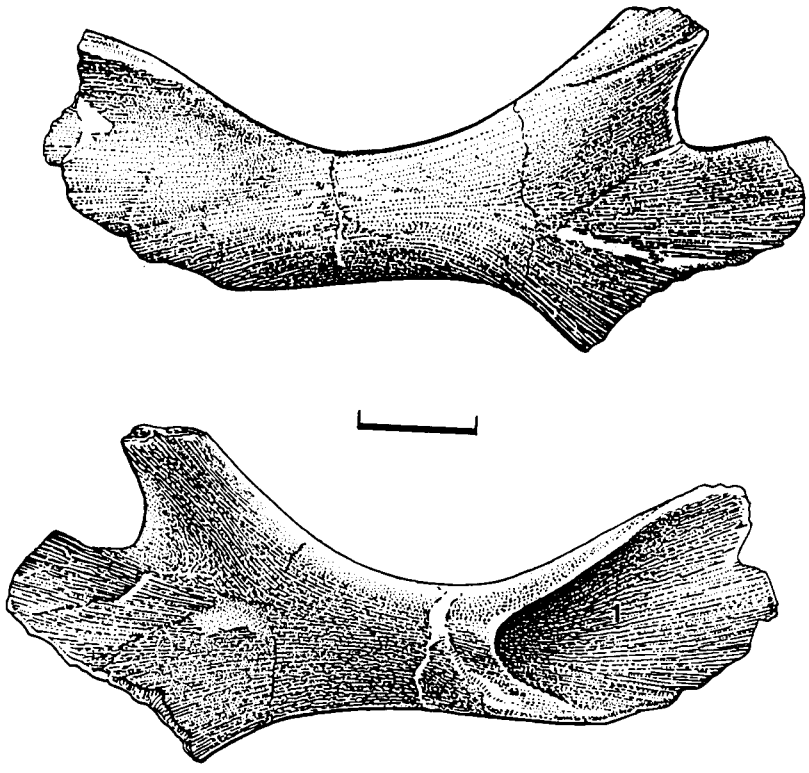

Figure 21.18. *Hypacrosaurus stebingeri*. RTMP 87.79.320. Left quadrate in posteromedial and lateral views. Scale = 5 mm.

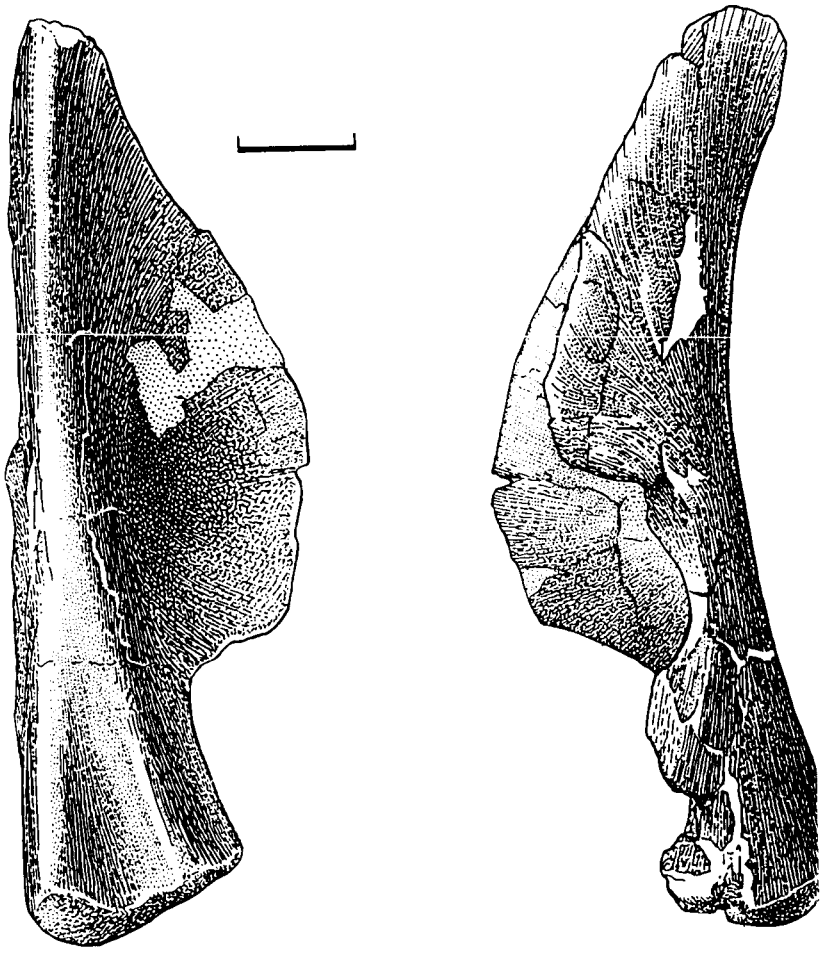

Figure 21.19. *Hypacrosaurus stebingeri*. RTMP 87.79.333. Left postorbital in internal and external aspects. Squamosal contact (1); laterosphenoid articulation (2); frontal suture (3); orbital rim (4); upper temporal fenestra (5); lateral temporal opening (6). Scale = 5 mm.

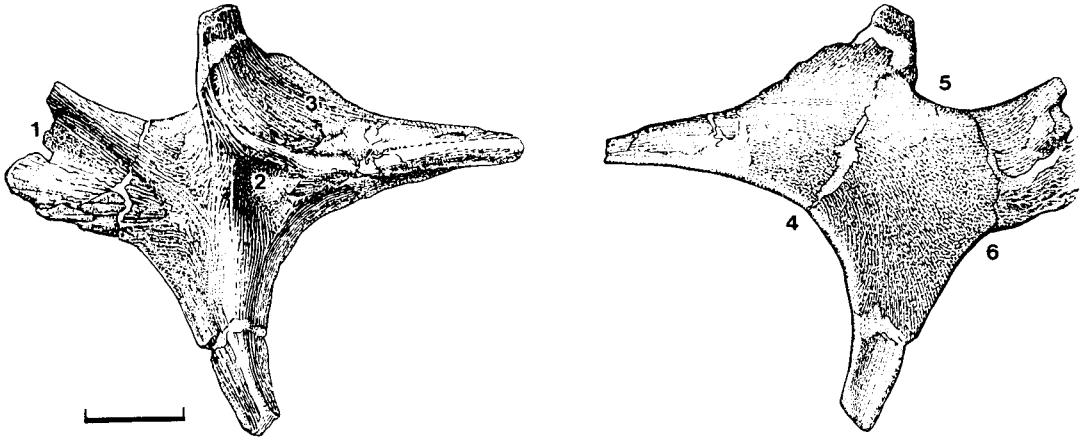

The humerus (Fig. 21.25D) is relatively stout compared to more mature specimens, but the deltopectoral crest has similar proportions to that of the adult. The ulna and radius (Fig. 21.25E) are longer than the humerus and proportionally more massive than the corresponding adult elements. Metacarpals III (Fig. 21.25F) and IV are slightly less than half the length of the radius. The elements of the manus are all very well ossified and are not

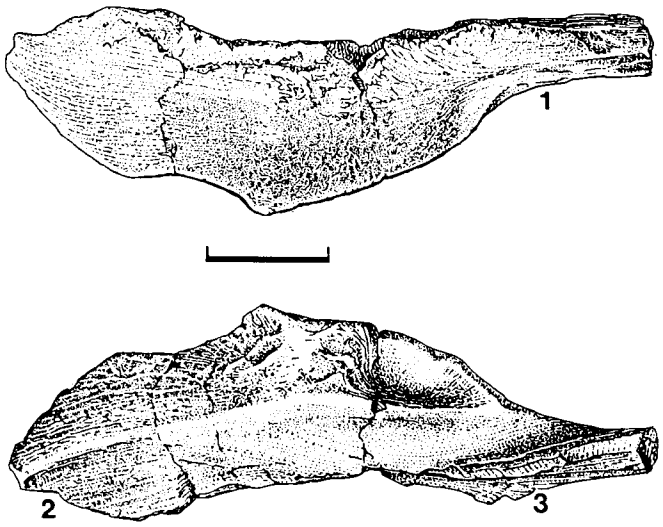

Figure 21.20. *Hypacrosaurus stebingeri.* RTMP 87.77.92. Left prefrontal in external and medial views. Orbital rim (1); frontal contact (2); nasal suture (3). Scale = 5 mm.

Figure 21.22. *Hypacrosaurus stebingeri.* MOR 548. **A.** Right dentary in medial view. **B.** Predentary in dorsal aspect. **C.** Right surangular in lateral view. **D.** Left surangular in dorsal aspect. Scale = 4 cm.

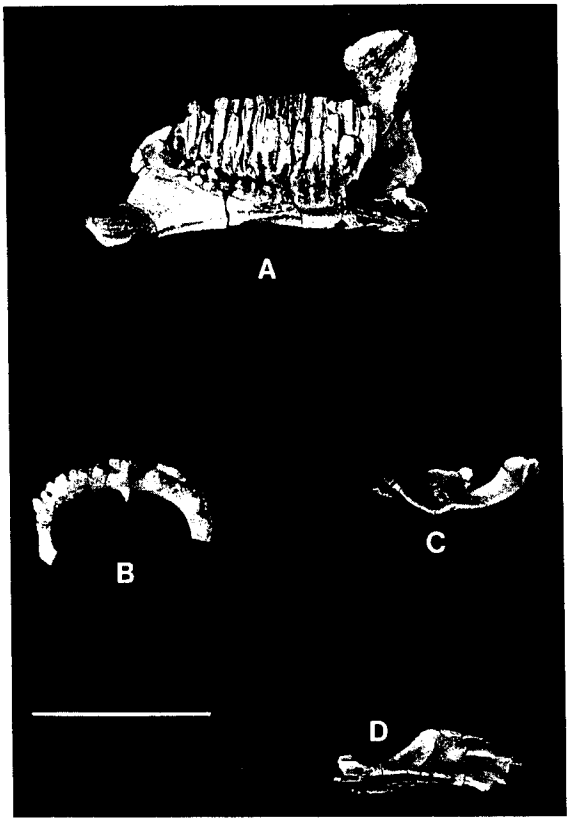

Figure 21.21. *Hypacrosaurus stebingeri.* RTMP 87.79.247. Left ectopterygoid in medial and dorsal views. Scale = 5 mm.

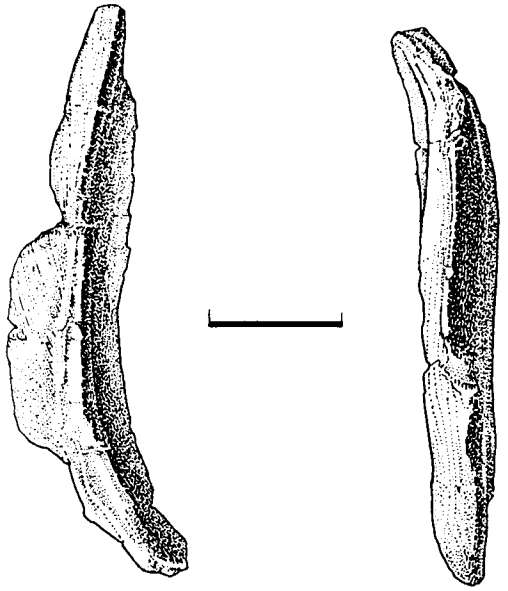

different from those of other lambeosaurids. Nothing was found that could be identified as a carpal element.

Within the embryonic pelvic girdle, the ilium is elongate and shallow dorsoventrally. Angulation between the anterior and posterior processes is minimal, but the antitrochanter is well developed. The nestling ilium (Fig. 21.26B) is similar to that of the adult. The ischium of the embryo has an expanded distal end, but it lacks the characteristic foot seen in the nestlings (Fig. 21.26C) and adults. The embryonic pubis is similar to that of the nestling (Fig. 21.26D,E), although the anterior blade is much narrower dorsoventrally. The anterior blade becomes deeper with maturity.

The femur, tibia, fibula, tarsals (including the distal tarsal), and pes elements of both the embryos and nestlings are of similar morphology to the adults. However, the nestling femora (Fig. 21.27A) do however, have a much more defined muscle scar medial to the fourth trochanter than do those of more mature individuals. The nestling tibia (Fig. 21.27B) and fibula (Fig. 21.27C) are similar in morphology to those of adults but are much more robust. Length-to-midshaft-circumference proportions of the femur and tibia change during growth (Table 21.1). Both the femur and tibia are more robust in the younger individuals than in the adults. This may have to do with the large cartilaginous caps that

Figure 21.23. *Hypacrosaurus stebingeri*. RTMP 87.79.266. Left mandible in lateral and medial aspects. Abbreviations: ar, articular; d, dentary; sa, surangular; sp, splenial. Scale = 10 mm.

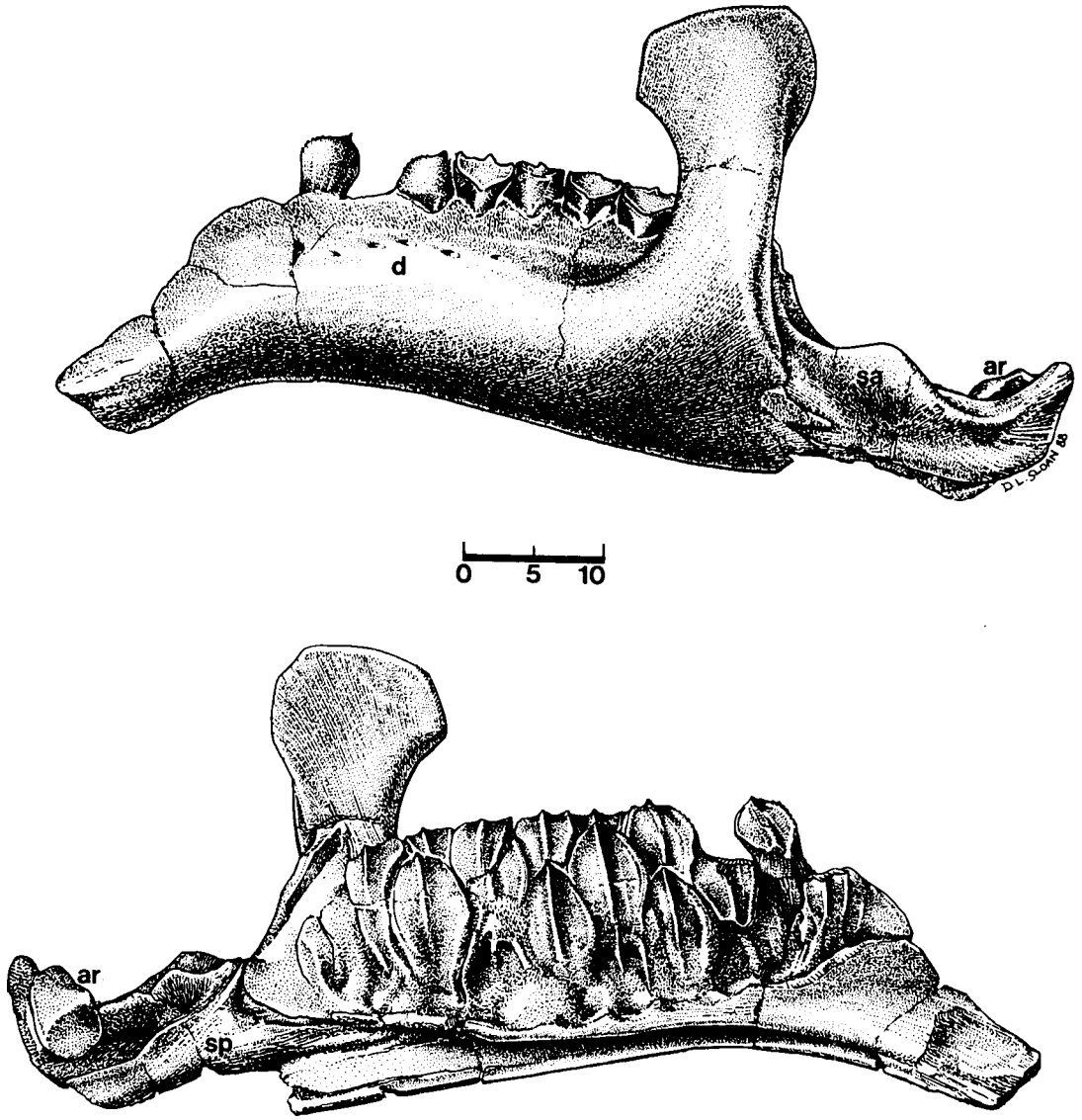

apparently existed at the ends of these elements, as explained below.

The embryonic and nestling astragalus (Fig. 21.27D) and calcaneum (Fig. 21.27E) are well ossified and morphologically similar to corresponding adult elements. The nestling metatarsals are slightly more robust than those of adults. Nestling phalanges, including the unguals (Fig. 21.27H), are nearly identical to those of adults.

Ossified tendons are present in embryonic individuals (RTMP 88.121.35). The tendons are highly vascularized, and were apparently very flexible during this period.

Osteohistology

Histologically, the cortex of embryonic bone (MOR 559) is highly vascularized, contains abundant osteocyte lacunae (Fig. 21.28A), and has little or no fibrous structure (Fig. 21.28B). Primary osteons are in their initial stages of development. The nestling bone is also highly vascularized, with abundant osteocyte lacunae (Fig. 21.28C), but has better developed primary osteons (Fig. 21.27D). However, the primary osteons are not fully developed. The bone is fibrolamellar in structure.

All of the articular surfaces of the appendicular skeleton of the embryos are incomplete. Abundant calcified cartilage columns are found at the ends of these bones. In the nestlings, these surfaces are more complete but still have abundant calcified cartilage columns. The incomplete ends of the bones of the embryos suggests there were large cartilage cones at all joints and ends of bones (Horner & Weishampel, 1988). Calcified cartilage is also abundant at all articular joints and union surfaces in the skull. The surfaces of the bones have a very

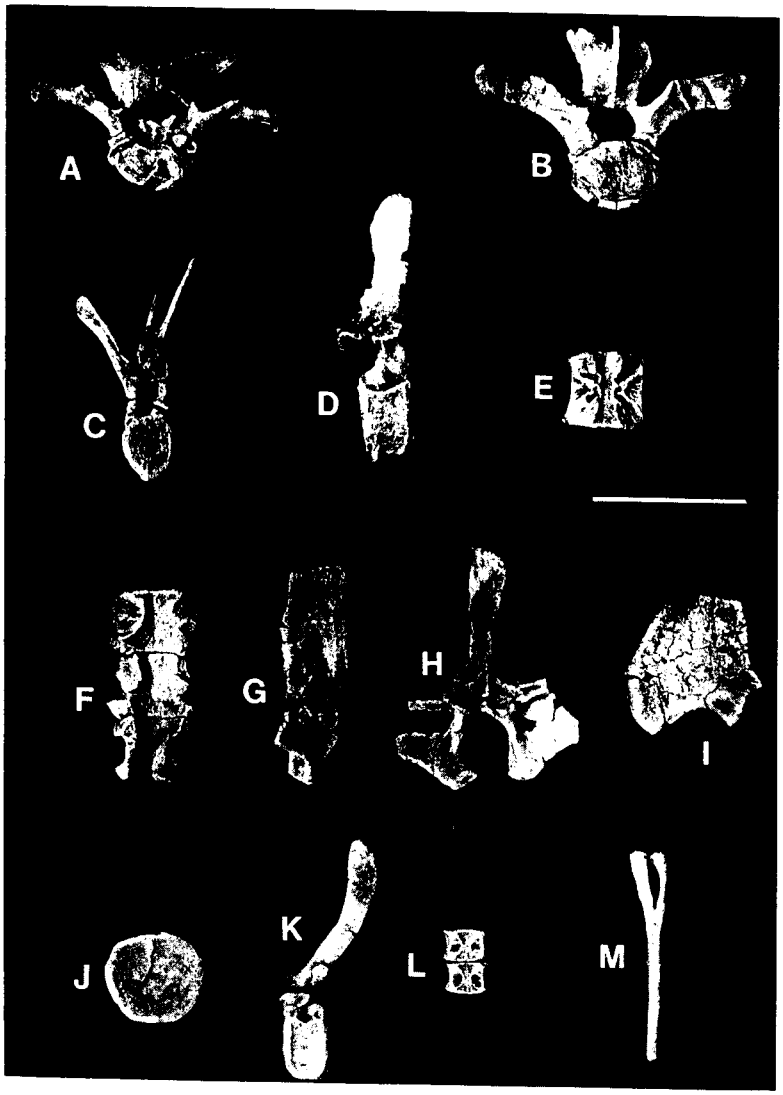

Figure 21.24. *Hypacrosaurus stebingeri*. MOR 548. **A, B**. Anterior views of cervical vertebrae. **C**. Anterior view of dorsal vertebra. **D**. Lateral view of dorsal vertebra. **E**. Dorsal centrum in dorsal aspect. **F**. Dorsal view of three sacral centra. **G, H**. Lateral and anterior views of sacral neural arch. **I**. Dorsal view of sacral rib. **J**. Posterior view of anterior caudal centra. **K**. Left lateral view of caudal vertebra. **L**. Two articulated distal caudals in dorsal view. **M**. Anterior view of a haemal arch. Scale = 4 cm.

coarse texture, with numerous vascular canals exiting on the surface, indicating very active growth at the periosteum. The combination of highly vascularized, fibrolamellar bone with an abundance of calcified cartilage indicates that these baby dinosaurs were growing very rapidly before their deaths (Ricqles, 1976; Currey, 1984).

It is unclear whether or not the femora and tibiae of the babies had different proportions than those of the adults. It may be that with the addition of the extensive cartilaginous caps at the ends of the baby bones, their proportions would have been the same as adults.

Figure 21.25. *Hypacrosaurus stebingeri*. MOR 548. **A, B**. Right scapula (A) and coracoid (B) in lateral views. **C**. Right sternal from anterior. **D**. Right humerus in lateral aspect. **E**. Right ulna and radius in medial view. **F**. Metacarpal III. **G**. Manus phalange. **H**. ungual phalange. Scale = 10 cm.

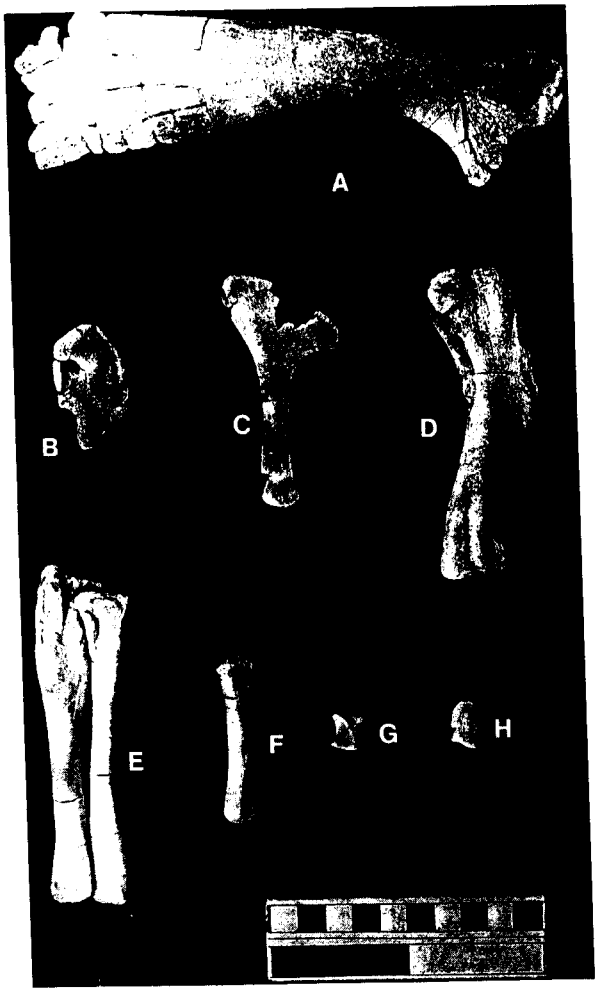

Early ontogeny

The most noticeable change that take place during the early ontogeny of *Hypacrosaurus stebingeri* (Appendix 21.1) occur in the skull due to the early development of the nasal crest. During development from the embryonic stages to the large nestling stage, the nasal crest domes slightly and the S-loop narial passage begins formation. Continued changes result in increased skull size as the crest vaults vertically. Most of the other cranial elements retain their overall morphology throughout ontogeny. The orbits remain proportionally large, but steadily decrease with size, and the snout remains short and highly angled. New tooth rows are added to both the maxilla and dentary, and there is most likely an addition of a least one tooth to each vertical row.

In the postcranial skeleton, the sutural facets of the vertebral centra and their respective neural arches become more rugose. The neural canal becomes proportionally smaller as the neural spines increase in height. The femur and tibia become less robust, a trend that continues until maturity. The ends of all bones ossify, and the processes and muscle scars become more distinct. The ossified tendons become more compact and therefore less flexible.

Phylogenetic considerations

It may be of phylogenetic importance that the premaxilla and nasal of the embryos possess no distinctive characters that would lead to the conclusion that lambeosaurids were derived from the hadrosaurids. The folds in the dorsal and ventral posterior processes of the premaxilla are apparently formed before ossification. All cranial elements of the embryos and nestlings possess each of the characters found in adult lambeosaurids. The embryos, therefore, offer no new data that would help to disprove the hypothesis that the classic "Hadrosauridae" are polyphyletic (Horner, 1990).

Discussion

The cranial elements of both the embryonic and nestling individuals of *Hypacrosaurus stebingeri* clearly show that the premaxillae/nasal crest of lambeosaurids was the major component that changed during ontogeny. Other changes include increase in the number of teeth, decrease in the relative proportion of the orbit, deepening and thickening of sutural rugosities, histological development, and possibly negative allometry in the femora and tibiae. Most other cranial and postcranial elements underwent few changes (Figs. 21.29 and 21.30). The small, slightly modified nasal capsules of the babies most likely allowed for higher frequencies of vocalization and facilitated communication with the adults, as suggested by Weishampel (1981b).

The embryonic and nestling specimens of *Hypacrosaurus stebingeri* described represent the largest col-

lection of baby skeletal material of any single species of "hadrosaur" known from any area in the world. Continued work with these specimens and the more mature individuals of the species promises to yield a much clearer understanding of individual variation, development, and growth in this species.

Acknowledgments

We thank Kevin Aulenback (RTMP) for preparation of the embryonic material, and Carrie Ancell (MOR) for preparation of the nestling material. We also thank the Kashiwagi Museum of Nagano, Japan, for making specimens and casts of juvenile material available for comparative studies. We would also like to thank the Tribal Council of the Blackfeet Nation for access to tribal lands, and Seldon Frisbee, Wally Bradley, and Ricky Reagan for access to their deeded or leased lands. Figures 21.3 and 21.4 were made by one of us (Currie), and Donna Sloan (RTMP) did the remaining embryonic illustrations. Terry Panasuk (MOR) photographed the nestlings. Funding for JRH was provided by NSF Grant No. EAR 8705986 and the Museum of the Rockies. Funding for PJC was derived from the Royal Tyrrell Museum of Palaeontology.

References

Andrews, R. C. 1932. *The New Conquest of Central Asia*, Vol. 1. (New York: American Museum of Natural History).

Figure 21.26. *Hypacrosaurus stebingeri*. MOR 548. **A–C**. Dorsal rib (A), left ilium (B), and ischium (C) in lateral views. **D, E**. Left pubis in medial (D) and lateral (E) views. Scale = 4 cm.

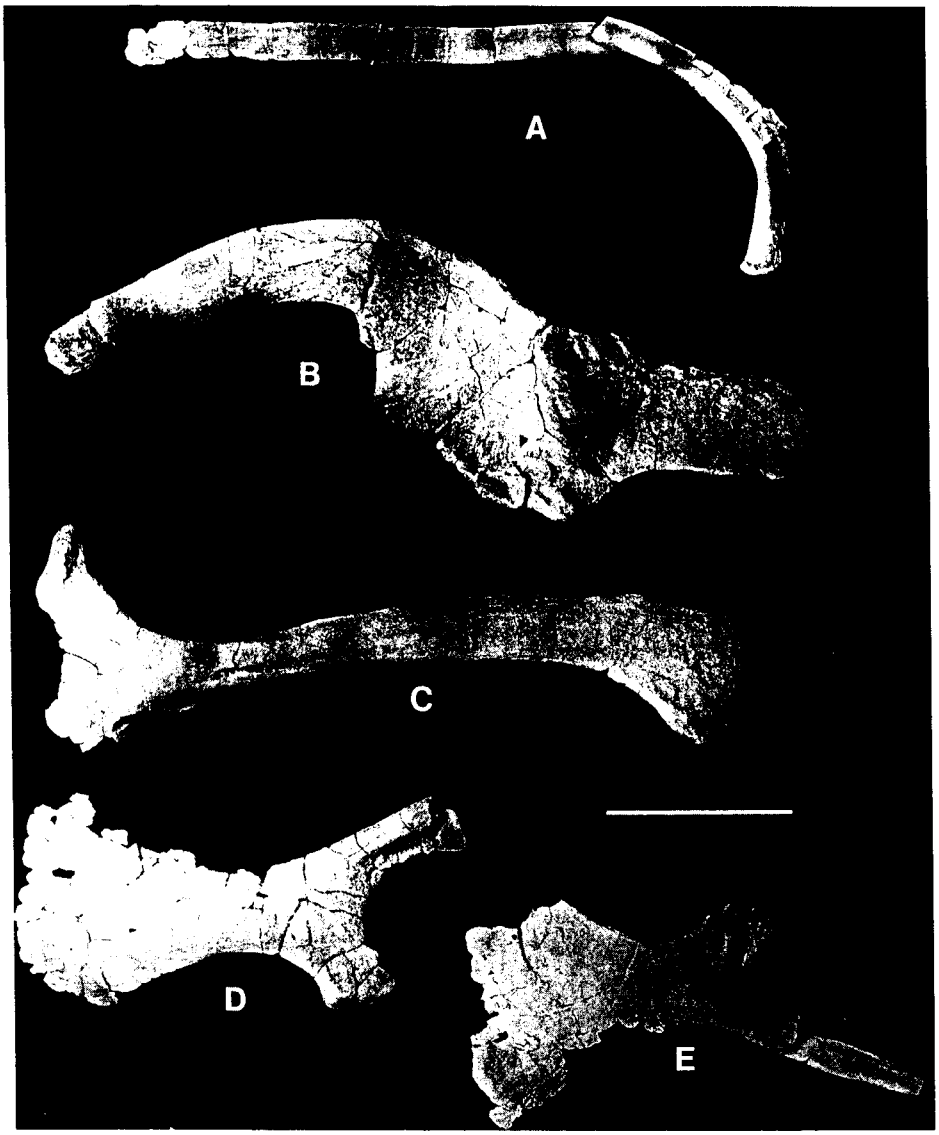

Brown, B. 1913. A new trachodont dinosaur, *Hypacrosaurus*, from the Edmonton Cretaceous of Alberta. *American Museum of Natural History Bulletin* 32: 395–406.

Brown, B., & Schlaikjer, E. M. 1940. The structure and relationship of *Protoceratops*. *Annals of the New York Academy of Sciences* 40: 133–266.

Currey, J. 1984. *The Mechanical Adaptations of Bone*. (Princeton: Princeton University Press).

Currie, P. J. & Horner, J. R. 1988. Lambeosaurine hadrosaur embryos (Reptilia: Ornithischia). *Journal of Vertebrate Paleontology* 8 (Supplement to No. 3): 13A.

Dodson, P. 1975. Taxonomic implications of relative growth in lambeosaurine hadrosaurs. *Systematic Zoology* 24: 37–54.

Fiorillo, A. R. 1987. Significance of juvenile dinosaurs from Careless Creek Quarry (Judith River Formation), Wheatland County, Montana. *In* P. J. Currie & E. H. Koster (eds.), *Fourth Symposium Mesozoic Terrestrial Ecosystems*. (Drumheller: Tyrrell Museum of Palaeontology), pp. 88–95.

Gilmore, C. W. 1917. *Brachyceratops*, a ceratopsian dinosaur from the Two Medicine Formation of Montana, with notes on associated fossil reptiles. *U.S. Geological Survey Professional Paper* 103: 1–45.

1924. On the skull and skeleton of *Hypacrosaurus*, a helmet-crested dinosaur from the Edmonton Cretaceous of Alberta. *Geological Survey of Canada Bulletin* 38: 49–64.

1937. On the detailed skull structure of a crested hadrosaurian dinosaur. *U.S. National Museum Proceedings* 84: 481–91.

Heaton, M. J. 1972. The palatal structure of some Canadian Hadrosauridae (Reptilia: Ornithischia). *Canadian Journal of Earth Sciences* 9: 185–205.

Horner, J. R. 1982. Evidence of colonial nesting and 'site fidelity' among ornithischian dinosaurs. *Nature* 297: 675–6.

1983. Cranial osteology and morphology of the type specimen of *Maiasaura peeblesorum* (Ornithischia: Hadrosauridae), with discussion of its phylogenetic position. *Journal of Vertebrate Paleontology* 3: 29–38.

1990. Evidence of diphyletic origination of the hadrosaurian (Reptilia: Ornithischia) dinosaurs. *In* K. Carpenter & P. J. Currie (eds.), *Dinosaur Systematics, Approaches and Perspectives*. (New York: Cambridge University Press), pp. 179–87.

1992. Cranial morphology of *Prosaurolophus* (Ornithischia; Hadrosauridae) with descriptions of two new hadrosaurid species, and an evaluation of hadrosaurid phylogenetic relationships. *Museum of the Rockies Occasional Paper* 2: 1–120.

Horner, J. R., & Makela, R. 1979. Nest of juveniles provides evidence of family structure among dinosaurs. *Nature* 282: 296–8.

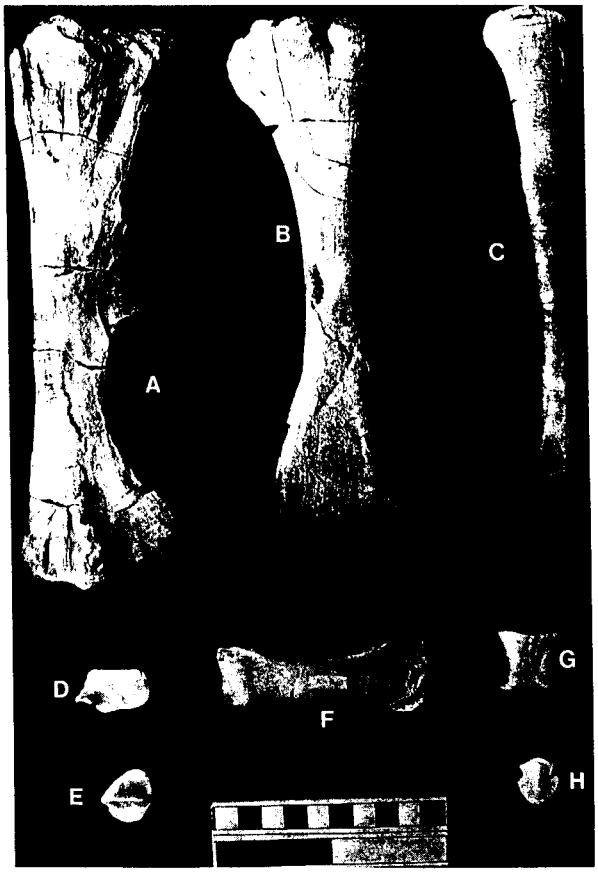

Figure 21.27. *Hypacrosaurus stebingeri*. MOR 548. **A, B**. Left femur (A) and tibia (B) in posterior views. **C**. Left fibula in medial view. **D, E**. Right astragulas (D) and left calcanium (E) in dorsal aspect. **F**. Left metatarsal III in anterior view. **G**. Left first phalange III in dorsal view. **H**. Ungual phalange from the pes in dorsal aspect. Scale = 10 cm.

Horner, J. R., Varricchio, D., & Goodwin, M. 1992. Marine transgressions and the evolution of Cretaceous dinosaurs. *Nature* 358: 59–61.

Horner, J. R. & Weishampel, D. B. 1988. A comparative embryological study of two ornithischian dinosaurs. *Nature* 332: 256–7.

Jepsen, G. L. 1964. Riddles of the terrible lizards. *American Scientist* 52: 227–46.

Langston, W., Jr. 1960. The vertebrate fauna of the Selma Formation of Alabama. Part VI. The dinosaurs. *Fieldiana: Geology Memoirs* 3: 319–63.

Lull, R. S. and Wright, N. E. 1942. Hadrosaurian dinosaurs of North America. *Geological Society of America Special Papers* 40: 1–242.

Morris, W. J. 1978. *Hypacrosaurus altispinus*? Brown from the Two Medicine Formation, Montana, a taxonomically indeterminate specimen. *Journal of Paleontology* 52: 200–5.

Table 21.1. Length-to-midshaft-circumference ratios for ontogenetic series of femora and tibiae of *Hypacrosaurus stebingeri*

Specimen numbers	Length (mm)	Length/circumference ratio
Embryonic femora		
RTMP 87.79.265	62.5	2.00:1
RTMP 89.79.52	68	2.00:1
MOR 562	80	2.00:1
RTMP 87.79.219	84	2.10:1
Nestling femora		
MOR 548-F1	168	2.25:1
MOR 548-F2	195	2.32:1
MOR 548.F3	235	2.35:1
Juvenile femur		
MOR 35	600	2.40:1
Subadult femur		
MOR 553	870	2.61:1
Adult femur		
MOR 549 (holotype)	1,050	2.75:1
Embryonic tibiae		
RTMP 87.79.113	66	2.76:1
RTMP 87.79.115	79	2.35:1
MOR 562	80	2.28:1
RTMP 87.79.114	81	2.25:1
Nestling tibiae		
MOR 548-T1	140	2.33:1
MOR 548-T2	180	2.57:1
MOR 548-T3	220	2.77:1
Juvenile tibia		
MOR 355-8-26-5-8	600	3.19:1
Adult tibia		
MOR 355-8-25-5-4	1,060	3.31:1

Ostrom, J. H. 1961. Cranial morphology of the hadrosaurian dinosaurs. *American Museum of Natural History Bulletin* 122: 33–186.

Ricqles, A. de. 1976. On bone histology of fossil and living reptiles, with comments on its functional and evolutionary significance. *In* A. d'A. Bellairs & C. B. Cox (eds.), *Morphology and Biology of Reptiles*. (London: Academic Press), pp. 123–50.

Sochava, A. V. 1972. The skeleton of an embryo in a dinosaur egg. *Paleontological Journal* 6: 527–31.

Sternberg, C. M. 1955. A juvenile hadrosaur from the Oldman Formation of Alberta. *National Museum of Canada Bulletin* 136: 120–2.

Weishampel, D. B. 1981a. The nasal cavity of lambeosaurine hadrosaurids (Reptilia: Ornithischia): Comparative anatomy and homologies. *Journal of Paleontology* 55: 1046–57.

Weishampel, D. B. 1981b. Acoustic analyses of potential vocalization in lambeosaurine dinosaurs (Reptilia: Ornithischia). *Paleobiology* 7: 252–61.

Weishampel, D. B., & Horner, J. R. 1990. Hadrosauridae. *In* D. B. Weishampel, P. Dodson, & H. Osmolska (eds.), *The Dinosauria*. (Berkeley: University of California Press), pp. 534–61.

Appendix 21.1. Diagnosis for *Hypacrosaurus stebingeri* n. sp. with discussion

Family Lambeosauridae (Horner, 1990)
Genus *Hypacrosaurus*; Brown 1913
Hypacrosaurus stebingeri, new species

Holotype

MOR 549, nearly complete skeleton, (Fig. 21.31).

Referred specimens

AMNH 5461, MOR 355, 455, 548, 553 (in part), 559 and 562; RTMP 88.79.36, 89.79.52, 87.79.22, 89.79.53 (for a more complete list of RTMP specimens see Appendix 21.2) and USNM 7948 and 11893.

Type locality

TM-065, Badger Creek, Glacier County, Montana.

Stratigraphic horizon

Upper Two Medicine Formation.

Age

Upper Cretaceous (Upper Campanian).

Etymology

stebingeri, to honor the late Eugene Stebinger, who first described the Two Medicine Formation and discovered the first remains of this species.

Diagnosis

This species has no autapomorphies. With *Hypacrosaurus altispinus* it shares a restricted external naris, wide narial crest, and restricted dorsal centra with very tall neural spines. With species of *Lambeosaurus* it shares a narial crest, the majority of which is composed of the premaxillae. *Hypacrosaurus stebingeri* has a long thin lacrimal intermediate in morphology between species of *Lambeosaurus* and *Hypacrosaurus altispi-*

Figure 21.28. *Hypacrosaurus stebingeri*. Histological sections of embryonic cortex (A, B) of femur (MOR 559), and nestling cortex (C, D) of femur (MOR 548). **A**. Section showing tremendous vascularization of the embryo. **B**. Section showing unorganized nature of embryonic bone. **C, D**, Sections showing woven bone and much more organized and oriented around vascular canals. Scale of A and C = 1 mm; of B and D = 0.5 mm.

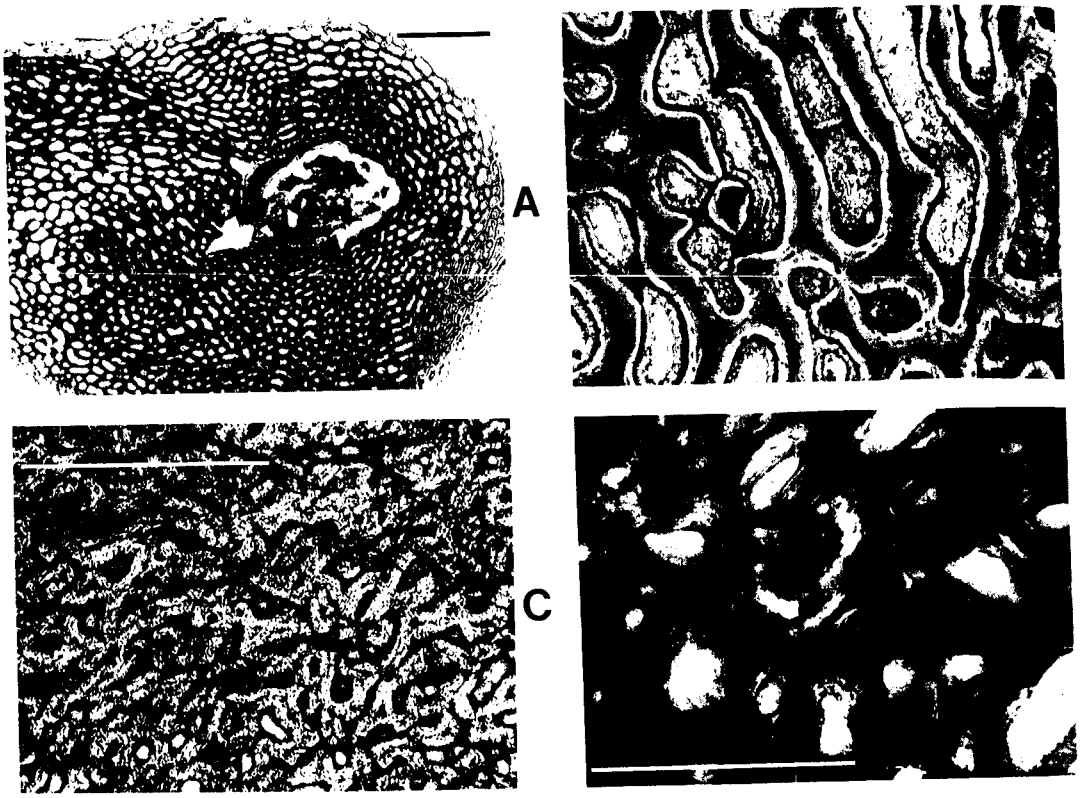

Figure 21.29. *Hypacrosaurus stebingeri*. Reconstructed composite skeleton of embryo (RTMP 88.3.2). Scale = 5 cm.

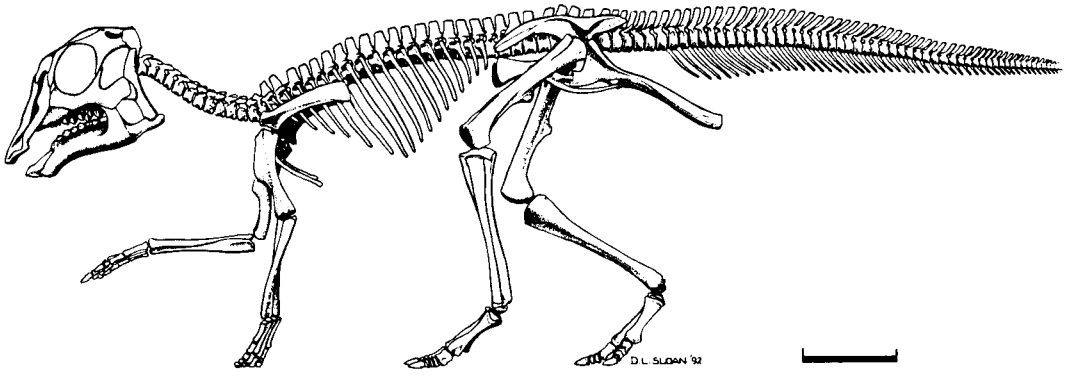

Figure 21.30. *Hypacrosaurus stebingeri*. Reconstructed skeleton of nestling (MOR 548). Scale = 21 cm.

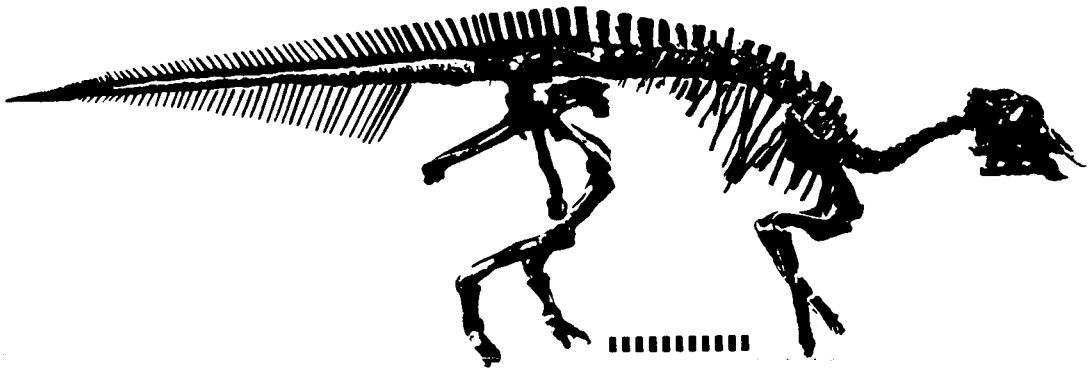

Figure 21.31. *Hypacrosaurus stebingeri*. MOR 549. **A–D**. Holotype skull in lateral view (A), left ilium in lateral aspect (B), and middorsal vertebra in anterior (C) and lateral (D) views. Scale in centimeters.

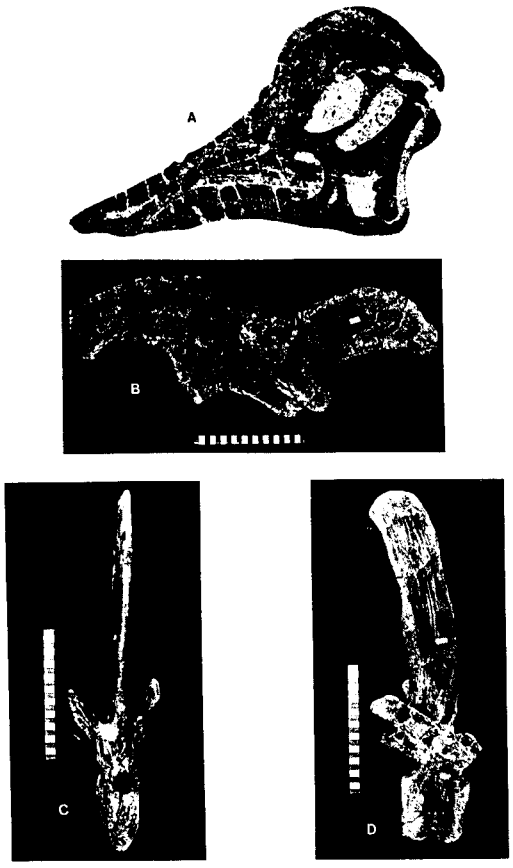

nus, and also has a narial crest with its apex directly over the anterior ends of the orbits, similar to the two latter taxa.

Discussion

Hypacrosaurus stebingeri is an unusual dinosaur taxon in that it has no autapomorphies. Phylogenetically, it appears to be an intermediate stage in the evolution of *Lambeosaurus* from the Judith River Formation to *Hypacrosaurus altispinus* from the Horseshoe Canyon Formation (Horner, Varricchio, & Goodwin, 1992). Interestingly, in juvenile specimens of *H. stebingeri* the anterior end of the nasal branch, where it meets the premaxilla, is bifurcated in a manner similar to species of *Corythosaurus*. More mature individuals of *H. stebingeri*, however, indicate a greater expansion of the premaxilla, whereas in *Corythosaurus* juveniles and subadults there is greater expansion of the nasal. Without the ontogenetic stages of these lambeosaurid taxa it would be difficult to identify some juveniles to genus and species even with an attempt as rigorous as that by Dodson (1975).

A specimen of *Hypacrosaurus altispinus*? was reported from the Two Medicine Formation of Montana by Gilmore (1917). Morris (1978) stated that there was not enough cranial material to verify whether or not Gilmore's specimen belonged to *Hypacrosaurus*, and suggested that it might instead be a species of *Lambeosaurus*. Whether coincidental or not, it is interesting that MOR 549 indicates a close relationship between *Lambeosaurus* and *Hypacrosaurus* as suggested by Morris. This conclusion stands in contrast to that of Lull and Wright (1942) that *Hypacrosaurus* was more closely related to *Corythosaurus* because the narial crests appear similar. Gilmore's specimen was found at the same stratigraphic level as the holotype (MOR 549) and other referred specimens of *H. stebingeri* and is therefore referred to as *H. stebingeri*.

With regard to the stratigraphic positions of the two species of *Hypacrosaurus*, it should be noted that *H. stebingeri* postdates the known species of *Lambeosaurus*, but predates *Hypacrosaurus altispinus* (Horner et al., 1992). *H. stebingeri*

is placed in the genus *Hypacrosaurus* because it shares more characters with *Hypacrosaurus* than it does with *Lambeosaurus*.

APPENDIX 2 Specimens of *Hypacrosaurus stebingeri* from Devil's Coulee

Little Diablo's Hill, Nest No. 2

Four unprepared broken eggs with embryonic bone (RTMP 88.79.36). Disarticulated bones from at least three individuals found along the eroded edge of the nest (RTMP 89.79). A single associated individual from the nest (RTMP 89.79.52). Cranial material (* = from same individual): an almost complete skull with associated squamosal and lower jaws RTMP 89.79.52 (Fig. 21.4); articulated pair of premaxillae, *RTMP 87.79.334 (Fig. 21.15), *RTMP 87.79.370); five right maxillae, RTMP 87.79.108, .153, .155, .238, .306 and three left maxillae, RTMP 87.79.154, .286, *.336 (Fig. 21.16); left jugal, *RTMP 87.79.332 (Fig. 21.17) and right jugal. *RTMP 87.79.369; two left postorbitals, *RTMP 87.79.333 (Fig. 21.19), RTMP 87.79.364; two sets of parietals, RTMP 87.79.241 (Fig. 21.6), *RTMP 87.79.374, three left quadrates, RTMP 87.79.18, .77, *.320 (Fig. 21.18) and one right quadrate, RTMP 87.79.298; a left frontal, RTMP 87.79.206 (Fig. 21.8), a pair of frontals, *RTMP 87.79.371, .372; left exoccipital, *RTMP 87.79.307 (Fig. 21.9); left and two right exoccipitals, RTMP 87.79.158; left laterosphenoid, RTMP 87.79.227 (Fig. 21.12), right laterosphenoid, *RTMP 87.79.373, left and right prootic, RTMP 87.79.201, *.303; parasphenoid–basisphenoid, *RTMP 87.79.335 (Fig. 21.13); basioccipitals, RTMP 87.79.157 (Fig. 21.10), RTMP 87.79.193; predentary, *RTMP 87.79.263; pair of lower jaws, *RTMP 87.79.266 (Fig. 21.22, *RTMP 87.79.267; left dentary fragments, RTMP 87.79.50, 51, 52, 149, .150, .151; right dentary fragments, RTMP 87.79.53, .152, .253; left ectopterygoid, RTMP 87.79.247.

Little Diablo's Hill, Nest No. 3

Broken egg containing an articulated skeleton with skull, RTMP 87.79.22. Not yet prepared.

Little Diablo's Hill, Nest No. 5

Right prefrontal, RTMP 87.79.17; laterosphenoid, RTMP 87.79.16; right exoccipital, RTMP 87.79.18; right dentary, RTMP 87.79.6. Specimens small representing embryos arrested earlier in development.

Little Diablo's Hill, Nest RTMP 89.79.53

Specimens found several meters east and 25 cm higher than Nest No. 2. Eight eggs and probably more originally (Fig. 21.2). No bone present and CT scans of two eggs did not reveal any embryonic skeletons.

Little Diablo's Hill

Isolated eggs, RTMP 88.79.34, 35, found near Nests 2 and 5. Eggs may have washed out been expelled from these nests. No embryonic bones present in eggs, suggesting they may have been sterile.

North Baby Butte

Locality stratigraphically lower than Little Diablo's Hill. Left prefrontal, RTMP 87.77.92 (Fig. 20.20), three basioccipitals, RTMP 87.77.88, .89, .90; five dentary fragments RTMP 87.77.83, .84, .85, .86, .138.

Kiddie's Corner

Locality 100 m from and 10 m below Little Diablo's Hill. Fragments of a left jugal, RTMP 87.80.25; left dentary RTMP 87.80.26.